FENOC
FirstEnergy Nuclear Operating Company

5501 North State Route 2
Oak Harbor, Ohio 43449

Barry S. Allen
Vice President - Nuclear

419-321-7676
Fax: 419-321-7582

April 21, 2010
L-10-131

10 CFR 50.55a

ATTN: Document Control Desk
U.S. Nuclear Regulatory Commission
Washington, DC 20555-0001

SUBJECT:
Davis-Besse Nuclear Power Station
Docket No. 50-346, License No. NPF-3
Additional Information Regarding 10 CFR 50.55a Request RR-A34 for Alternative Repair Methods for Reactor Pressure Vessel Head Penetration Nozzles (TAC No. ME3703)

By correspondence dated April 1, 2010, FirstEnergy Nuclear Operating Company (FENOC) submitted 10 CFR 50.55a Request RR-A34, which requests Nuclear Regulatory Commission (NRC) approval of alternative methods to repair the reactor pressure vessel (RPV) penetration nozzles at the Davis-Besse Nuclear Power Station (DBNPS). By correspondence dated April 9, 2010, the NRC staff requested additional information to complete its review of RR-A34. Responses were provided by correspondence dated April 16, 2010.

In support of the NRC review of RR-A34, "DB-1 CRDM Nozzle J-Groove Weld Flaw Evaluation for IDTB Repair" is enclosed. The complete J-groove weld analysis contains proprietary information that is to be withheld from public disclosure pursuant to 10 CFR 2.390. Therefore, Enclosure A provides a nonproprietary version of the AREVA J-groove weld analysis for full public disclosure. Enclosure B contains the AREVA affidavit to support the disclosure request for the proprietary J-groove weld analysis, and Enclosure C provides the complete J-groove weld analysis that contains sections to be withheld from public disclosure.

A047
NRR

The proposed alternatives are to be implemented during the ongoing DBNPS maintenance and refueling outage. Therefore, as stated in the correspondence dated April 1, 2010, FENOC is requesting expedited NRC staff review and approval of the proposed alternative, RR-A34.

There are no regulatory commitments contained in this letter. If there are any questions, or if additional information is required, please contact Mr. Thomas A. Lentz, Manager – Fleet Licensing, at 330-761-6071.

Sincerely,

Barry S. Allen

Barry S. Allen

Enclosures:
A. DB-1 CRDM Nozzle J-Groove Weld Flaw Evaluation for IDTB Repair (Nonproprietary)
B. Affidavit for DB-1 CRDM Nozzle J-Groove Weld Flaw Evaluation for IDTB Repair
C. DB-1 CRDM Nozzle J-Groove Weld Flaw Evaluation for IDTB Repair (Proprietary)

cc: NRC Region III Administrator (Enclosure A only)
NRC Resident Inspector (Enclosure A only)
Nuclear Reactor Regulation Project Manager (Enclosure A only)
Utility Radiological Safety Board (Enclosure A only)

Enclosure A
L-10-131

DB-1 CRDM Nozzle J-Groove Weld Flaw Evaluation for IDTB Repair
(Nonproprietary)
(59 pages follow)

AREVA

CALCULATION SUMMARY SHEET (CSS)

Document No. 32 - 9136508 - 001 Safety Related: ☒ Yes ☐ No

Title DB-1 CRDM Nozzle J-Groove Weld Flaw Evaluation for IDTB Repair

PURPOSE AND SUMMARY OF RESULTS:

Purpose

This document is a non-proprietary version of AREVA NP Document 32-9134664-002. The AREVA NP proprietary information removed from 32-9134664-002 is indicated by a pair of braces "{ }".

The purpose of the present analysis is to determine from a fracture mechanics viewpoint the suitability of leaving degraded J-groove weld and butter material in the Davis Besse Unit 1 reactor vessel head following the repair of a Control Rod Drive Mechanism (CRDM) nozzle by the ID temper bead weld procedure. It is postulated that a small flaw in the head would combine with a large stress corrosion crack in the weld and butter to form a radial corner flaw that would propagate into the low alloy steel head by fatigue crack growth under cyclic loading conditions.

The purpose of Revision 1 is to change the indicator for removed proprietary information from square brackets "[ ]" to braces "{ }".

Summary of Results

Based on a combination of linear elastic and elastic plastic fracture mechanics analysis of a postulated remaining flaw in the original Alloy 182 J-groove weld and butter material, a Davis Besse Unit 1 CRDM nozzle is considered to be acceptable for at least 4 years of operation following an IDTB weld repair. The controlling loading condition was determined to be the rod withdrawal transient, for which it was shown that with safety factors of 3 on primary loads and 1.5 on secondary loads that the applied tearing modulus (11.63) was still less than the tearing modulus of the low alloy steel head material (12.93).

*This document consists of pages 1 – 46, A-1, B-1 – B-3, C-1 – C-4, D-1 – D-3, and E-1 – E-2.

THE FOLLOWING COMPUTER CODES HAVE BEEN USED IN THIS DOCUMENT:

CODE/VERSION/REV	CODE/VERSION/REV
ANSYS/10/0	

THE DOCUMENT CONTAINS ASSUMPTIONS THAT SHALL BE VERIFIED PRIOR TO USE

☐ YES
☒ NO

Review Method: ☒ Design Review (Detailed Check)
☐ Alternate Calculation

Signature Block

Name and Title (printed or typed)	Signature	P/R/A and LP/LR	Date	Pages/Sections Prepared/Reviewed/Approved
D. E. Killian Advisory Engineer		P	4/20/10	All
S. H. Mahmoud Engineer IV		R	4/20/10	All
T. M. Wiger Unit Manager		A	4/20/10	All

Note: P/R/A designates Preparer (P), Reviewer (R), Approver (A);
LP/LR designates Lead Preparer (LP), Lead Reviewer (LR)

Project Manager Approval of Customer References (N/A if not applicable)

Name (printed or typed)	Title (printed or typed)	Signature	Date
R. J. Baker, Jr.	Project Manager		4/20/10

Mentoring Information (not required per 0402-01)

Name (printed or typed)	Title (printed or typed)	Mentor to: (P/R)	Signature	Date
N/R				

Record of Revision

Revision No.	Date	Pages/Sections/ Paragraphs Changed	Brief Description / Change Authorization
000	04/2010	All	Original release
001	04/2010	Page 20	Changed yield and ultimate strengths in Table 4-1
		Pages 25-26	Pages reflect changes to Section 4.3 to enhance the description of the Rod Withdrawal Transient
		Pages 32-46	Calculations modified to account for changes to yield and ultimate strengths in Table 4-1
		Throughout	Added square brackets ("[ ]") to indicate removed proprietary information
002	04/2010	Throughout	Changed indicator for removed proprietary information from square brackets ("[ ]") to braces ("{ }")

Table of Contents

Page

SIGNATURE BLOCK 2

RECORD OF REVISION 3

LIST OF TABLES 6

LIST OF FIGURES 7

1.0 INTRODUCTION 8

2.0 ANALYTICAL METHODOLOGY 11

2.1 Stress Intensity Factor Solution 13

2.1.1 Finite Element Crack Model 13

2.1.2 Stress Mapping 13

2.1.3 Crack Growth Considerations 15

2.1.4 Plastic Zone Correction 15

2.2 Linear-Elastic Facture Mechanics 16

2.3 Elastic-Plastic Facture Mechanics 16

2.3.1 Screening Criteria 16

2.3.2 Flaw Stability and Crack Driving Force 16

3.0 ASSUMPTIONS 19

3.1 Unverified Assumptions 19

3.2 Justified Assumptions 19

3.3 Modeling Simplifications 19

4.0 DESIGN INPUTS 20

4.1 Materials 20

4.1.1 Mechanical and Thermal Properties 20

4.1.2 Reference Temperature 22

4.1.3 Fracture Toughness 22

4.1.4 J-integral Resistance Curve 22

4.1.5 Fatigue Crack Growth Rate 24

4.2 Basic Geometry 25

4.3 Operating Transients 25

4.4 Applied Stresses 26

Table of Contents
(continued)

Page

4.4.1 Residual Stresses 26
4.4.2 Operational Stresses 26

5.0 CALCULATIONS 31
5.1 Fatigue Crack Growth 31
5.2 LEFM Flaw Evaluations 35
5.3 EPFM Flaw Evaluations 36

6.0 SUMMARY OF RESULTS AND CONCLUSIONS 44
6.1 Summary of Results 44
6.2 Conclusion 44

7.0 REFERENCES 45

APPENDIX A : VERIFICATION OF COMPUTER CODE ANSYS A-1

APPENDIX B : COMPUTER FILES IN COLDSTOR B-1

APPENDIX C : FINITE ELEMENT CRACK MODEL C-1

APPENDIX D : FINITE ELEMENT STRESS MODEL D-1

APPENDIX E : STRESS INTENSITY FACTOR DUE TO PRESSURE E-1

List of Tables

Page

Table 1-1: Safety Factors for Flaw Acceptance 9
Table 4-1: Material Properties for Head 20
Table 4-2: Material Properties for Weld Metal 21
Table 4-3: Material Properties for Cladding 21
Table 4-4: Transient Analysis Time Points for Operational Stresses 30
Table 5-1: Flaw Growth and LEFM Evaluation 32
Table 5-2: EPFM Evaluation for Shutdown Conditions 38
Table 5-3: EPFM Evaluation for Heatup/Cooldown with Reactor Trip 39
Table 5-4: EPFM Evaluation for Rod Withdrawal Accident 40

List of Figures

Page

Figure 1-1: ID Temper Bead Weld Repair 10
Figure 2-1: Postulated Radial Flaw on Uphill Side 12
Figure 2-2: Finite Element Crack Model 14
Figure 4-1: Correlation of Coefficient, C, of Power Law with Charpy V-Notch Upper Shelf Energy 23
Figure 4-2: Correlation of Exponent, m, of Power Law with Coefficient, C, and Flow Stress, σ_o 23
Figure 4-3: DEI Finite Element Stress Model 27
Figure 4-4: DEI Finite Element Stress Model – Weld Region 28
Figure 4-5: Finite Element Stress Model for Operational Stresses 29
Figure 5-1: J-T Diagram for Shutdown Conditions 41
Figure 5-2: J-T Diagram for Heatup/Cooldown with Reactor Trip 42
Figure 5-3: J-T Diagram for Rod Withdrawal Accident 43

1.0 INTRODUCTION

A March 2010 inspection of Alloy 600 control rod drive mechanism (CRDM) nozzles in the reactor vessel closure head (RVCH) at Davis Besse Unit 1 revealed defects in several nozzles and nozzle-to-RVCH partial penetration welds, along with evidence of leakage as manifested by deposits of boric acid crystals on the outer surface of the head. The original RVCH at Davis Besse Unit 1 (DB-1) was replaced in 2002 with the closure head from a suspended Midland plant owned by Consumers Power Company. It is currently believed that the leakage in the DB-1 RVCH was caused by primary water stress corrosion cracking (PWSCC) of the susceptible Alloy 600 nozzles and Alloy 182 welds. Degraded nozzles at DB-1 are to be repaired using an inside diameter temper bead (IDTB) welding procedure wherein the lower portion of a nozzle is removed by a boring procedure and the remaining portion of the nozzle is welded to the low alloy steel reactor vessel head above the original Alloy 182 J-groove attachment weld, as shown in Figure 1-1. The repair is more fully described by the design drawing [1] and the design specification [2]. Although the remnant J-groove weld would no longer be associated with the primary pressure boundary, a defect in the weld could grow into the low allow steel RVCH and thereby impact the structural integrity of the remaining pressure boundary. Since a potential, or even detected, flaw in the J-groove weld can not be sized by currently available non-destructive examination techniques, it is assumed that the "as-left" condition of the remnant J-groove weld includes degraded or cracked weld material extending through the entire J-groove weld and Alloy 182 butter material.

Since it is known from analysis of the original Davis Besse Unit 1 CRDM reactor vessel head nozzle penetrations [3] that the hoop stress in the J-groove weld is greater than the axial stress at the same location, the preferential direction for cracking would be axial, or radial relative to the nozzle. Reference 3 also demonstrates that stresses tend to be higher on the uphill side of the nozzles than on the downhill side. It is postulated that a radial crack in the Alloy 182 weld metal would propagate by PWSCC, through the weld and butter, to the interface with the head material, where it is fully expected that such a crack would then blunt, or arrest, as discussed in Reference 4 for interfaces with low alloy steels. Since the height of the weld and butter along the bored surface is about 2" on the uphill side of the outermost CRDM nozzle, a radial crack depth extending from the corner of the weld to the low alloy steel head would be very deep. Although primary water stress corrosion cracking would not extend into the head, it is further postulated that a small fatigue initiated flaw forms in the low alloy steel head and combines with the stress corrosion crack in the weld to form a large radial flaw that would propagate into the head by fatigue crack growth under cyclic loading conditions. Linear-elastic (LEFM) and elastic-plastic (EPFM) fracture mechanics procedures are utilized to evaluate this worst case flaw in the original J-groove weld and butter.

Key features of the fracture mechanics analysis are:

- This analysis applies specifically to the CRDM nozzle penetrations in the Davis Besse Unit 1 reactor vessel closure head. A J-integral resistance curve is developed based on estimates of the Charpy V-notch upper-shelf energy for the DB-1 head plate material.
- Flaw growth is calculated for a 4 year period of operation, corresponding to 2 fuel cycles.
- Flaw acceptance is based on the available fracture toughness and ductile tearing resistance of the RVCH material considering the safety factors listed in Table 1-1.

Table 1-1: Safety Factors for Flaw Acceptance

Linear-Elastic Fracture Mechanics			
Operating Condition	Evaluation Method	Fracture Toughness / K_I	
Normal/Upset	K_{Ia} fracture toughness	$\sqrt{10} = 3.16$	
Emergency/Faulted	K_{Ic} fracture toughness	$\sqrt{2} = 1.41$	
Elastic-Plastic Fracture Mechanics			
Operating Condition	Evaluation Method	Primary	Secondary
Normal/Upset	J/T based flaw stability	3.0	1.5
Normal/Upset	$J_{0.1}$ limited flaw extension	1.5	1.0
Emergency/Faulted	J/T based flaw stability	1.5	1.0
Emergency/Faulted	$J_{0.1}$ limited flaw extension	1.5	1.0

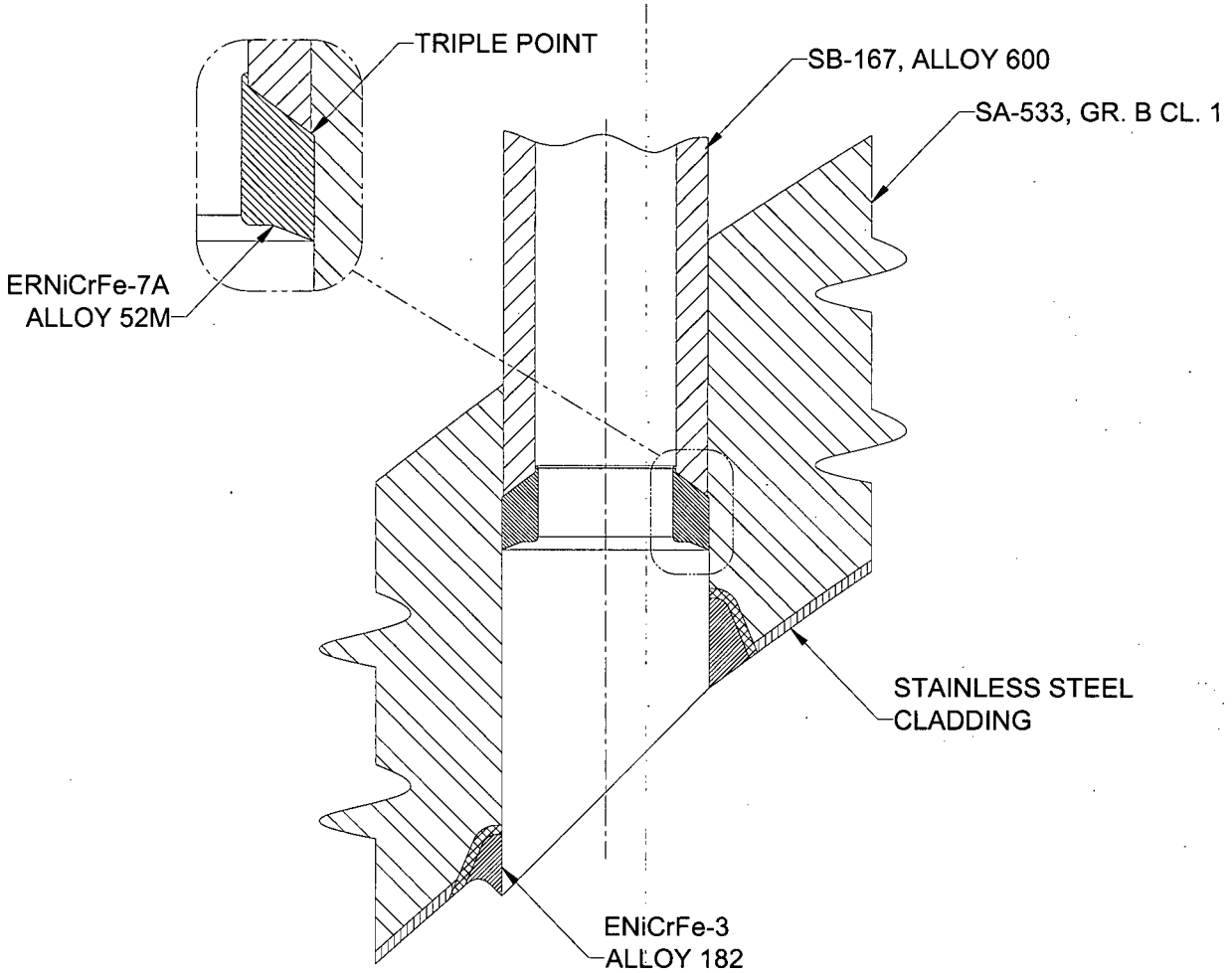

Figure 1-1: ID Temper Bead Weld Repair

2.0 ANALYTICAL METHODOLOGY

A radial flaw at the inside corner of non-radial head penetration is evaluated based on a combination of linear-elastic fracture mechanics (LEFM) and elastic-plastic fracture mechanics (EPFM), as outlined below.

1. Postulate a radial flaw in the J-groove weld, extending from the inside corner of the penetration to the interface between the butter and head, as shown in Figure 2-1 for the uphill side of the penetration. Previous analysis [5] has shown that even for large downhill welds, the controlling location is the uphill side of the penetration, due to higher stresses and the additional constraint provided by the acute angle between the material borders along the cladding and bore.

2. Develop a three-dimensional finite element crack model of the reactor vessel head in the vicinity of the outermost nozzle penetration, with crack tip elements along the interface between the Alloy 182 butter and the low alloy steel base metal. This crack model will be used to obtain stress intensity factors at various positions along the crack front for combined stresses due to J-groove welding, hydrostatic testing, nozzle removal, and transient loading conditions.

3. Develop a mapping procedure to transfer stresses from uncracked finite element stress analysis models (for residual and operational stresses) to the crack face of the crack model. This will enable stress intensity factors to be calculated for arbitrary stress distributions over the crack face utilizing the principle of superposition.

4. Calculate fatigue crack growth for cyclic loading conditions using combined residual and operational stresses from pressure and thermal loads. It is noted that the only effect of residual stress on fatigue crack growth is in the calculation of the R ratio, or K_{min}/K_{max}, which is the ratio of the minimum and maximum stress intensity factors for a pair of stress states. Starting from the stress intensity factor calculated by the finite element crack model for the initial flaw size, stress intensity factors are updated for each increment of crack growth by the square root of the ratio of the flaw sizes over the increment.

5. Utilize the screening criteria of ASME Code Section XI, Appendix H to determine the failure mode and appropriate method of analysis (LEFM or EPFM) for flaws in ferritic materials, considering the applied stress, temperature, and material toughness. For LEFM flaw evaluations, compare the stress intensity factor at the final flaw size to the available fracture toughness, with appropriate safety factors, as discussed in Section 2.2. When the material is more ductile and EPFM is the appropriate analysis method, evaluate flaw stability and crack driving force as described in Section 2.3.

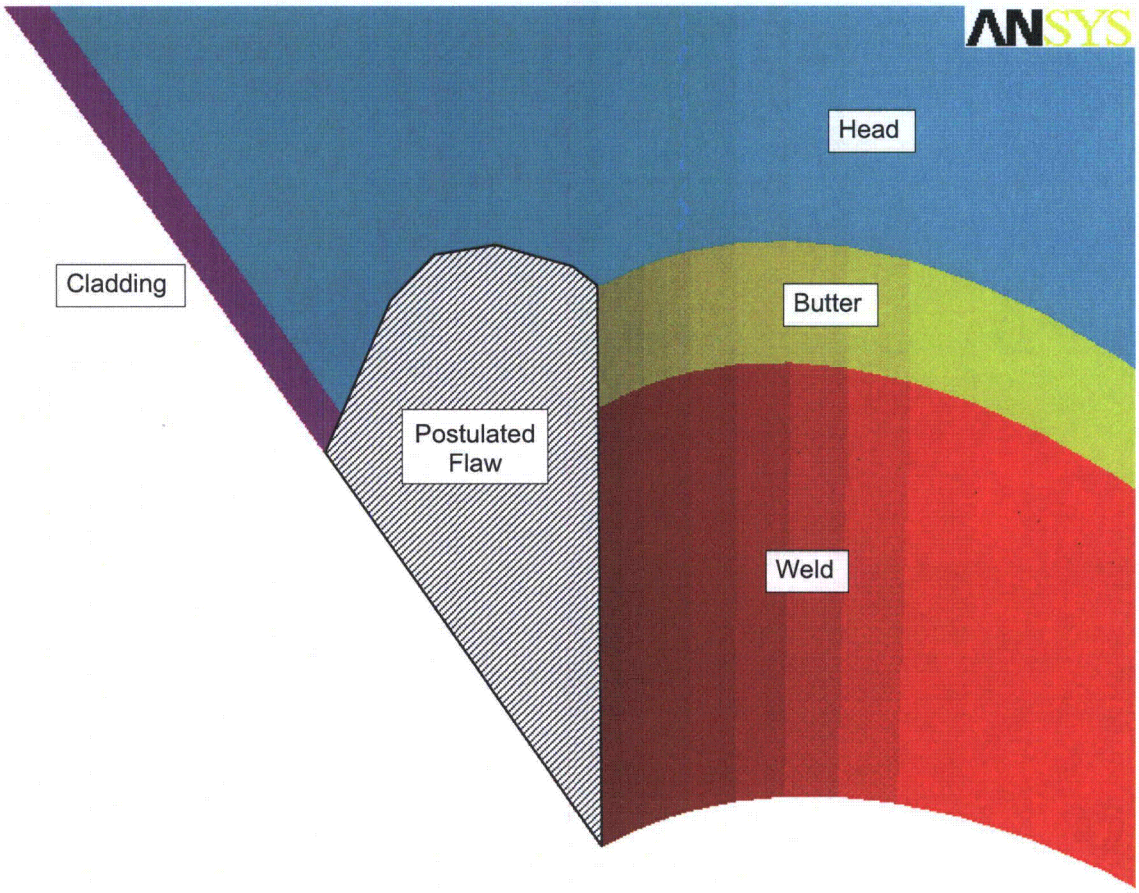

Figure 2-1: Postulated Radial Flaw on Uphill Side

2.1 Stress Intensity Factor Solution

Stress intensity factors for corner flaws at a non-radial nozzle penetration are best determined by finite element analysis using three-dimensional models with crack tip elements along the crack front. Although loads can be applied to finite element crack models like any other structural model, the crack model was developed to serve as a flaw evaluation tool that could accept stresses from separate stress analyses. This strategy makes it possible, for example, to obtain pressure and thermal stresses from an independent thermal/structural analysis and then transfer these stresses to a crack model for flaw evaluations. Using the principle of superposition common to fracture mechanics analysis, the only stresses that need be considered for these flaw evaluations are the stresses on the crack face. A mapping procedure is developed to transfer stresses from a separate stress analysis to the crack face of the crack model.

2.1.1 Finite Element Crack Model

A three-dimensional finite element model is developed for the reactor vessel head in the vicinity of the outermost nozzle penetration, by modeling a portion of the head, cladding, and butter with the ANSYS finite element computer program [6]. Since stresses increase with penetration angle, it is conservative to base the model on the outermost nozzle penetration. Details of the finite element crack models are presented in Appendix A.

The three-dimensional finite element model is first constructed to represent an unflawed non-radial nozzle penetration in the reactor vessel head using the ANSYS SOLID95 20-node structural element. Elements along the crack front are then replaced by a sub-model of crack tip elements along the interface between the Alloy 182 butter and the low alloy steel base metal. These elements consist of 20-node isoparametric elements that are collapsed to form a wedge with the appropriate mid-side nodes shifted to quarter-point locations to simulate a singularity at the crack tip. The final crack model is shown in Figure 2-2.

Stress intensity factors are obtained using the ANSYS KCALC routine at 10 positions along each crack front, as indicated in Figure 2-2. Position 1 in located on the cladding surface, Position 2 at the cladding/base metal interface, and Position 10 is at the bored surface in the head.

2.1.2 Stress Mapping

Residual and operational stresses, obtained from separate finite element models, are mapped onto the crack face of the finite element crack model shown in Figure 2-2 to calculate the individual contributions to the stress intensity factors. A set of ANSYS parametric design language instructions (macro) has been written based on the *MOPER,MAP command to transfer stresses by nodal interpolation from a dissimilar finite element model (e.g., residual stresses) to the crack model. Stresses from an identical finite element model (e.g., operational stresses), are simply copied from the stress model to the crack model.

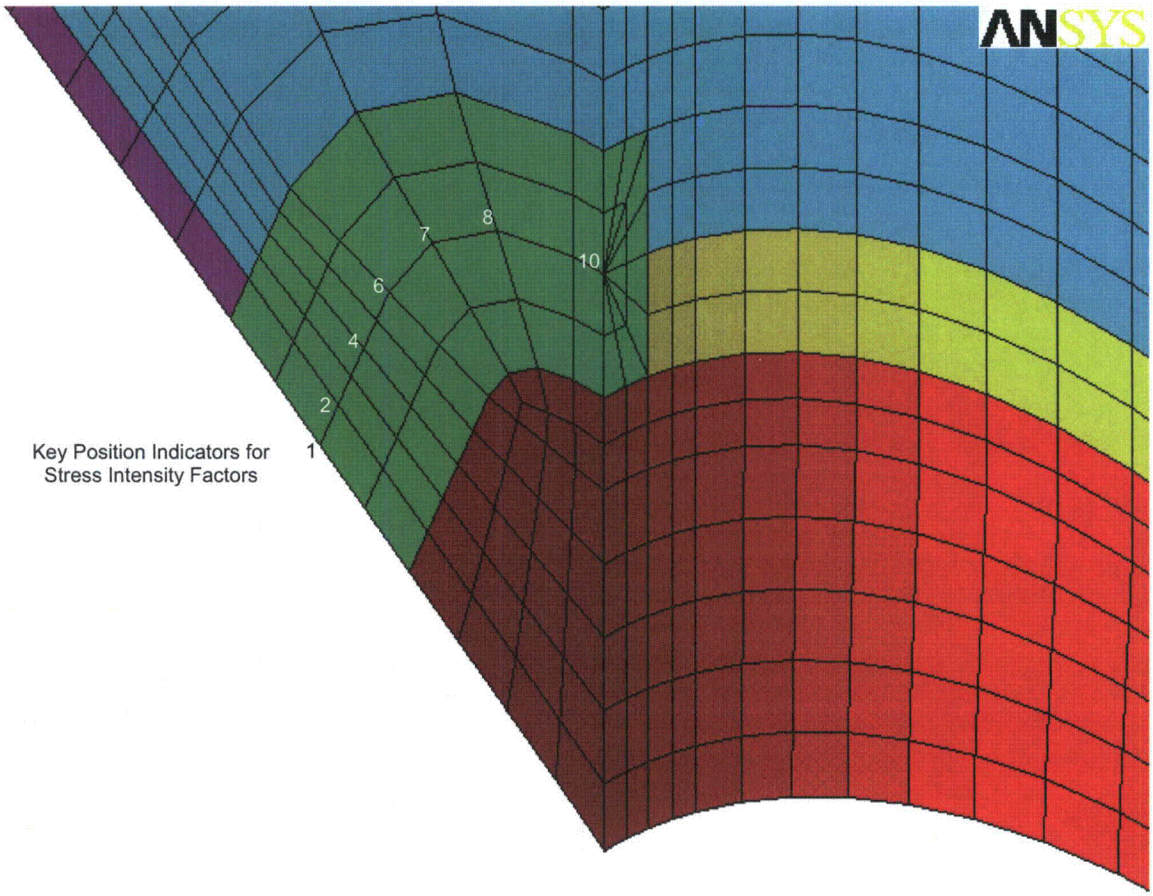

Figure 2-2: Finite Element Crack Model

2.1.3 Crack Growth Considerations

The fundamental expression for the crack tip stress intensity factor is

$$K_I = \sigma\sqrt{\pi a}$$

Since the crack model is developed for a single flaw size, stress intensity factors are updated at each increment of crack growth by the square root of the flaw size; i.e.,

$$K_I(a_{i+1}) = K_I(a)\sqrt{\frac{a_{i+1}}{a_i}},$$

where a = flaw size

i = increment of crack growth.

Since the stress intensity factor is directly proportional to the magnitude of the stress and both residual and operating stresses decrease in the direction of crack growth, this procedure produces conservative estimates of stress intensity factor as the crack extends into the head and stresses diminish over the expanding crack face.

2.1.4 Plastic Zone Correction

The Irwin plasticity correction is used to account for a moderate amount of yielding at the crack tip. For plane strain conditions, this correction is

$$r_y = \frac{1}{6\pi}\left(\frac{K_I(a)}{\sigma_y}\right)^2, \qquad \text{[Ref. [7] , Eqn. (2.63)]}$$

where $K_I(a)$ = stress intensity factor based on the actual crack size, a

σ_y = material yield strength.

A stress intensity factor, $K_I(a_e)$, is then calculated for an effective crack size,

$$a_e = a + r_y,$$

based on the same scaling technique utilized for crack growth; i.e.,

$$K_I(a_e) = K_I(a)\sqrt{\frac{a_e}{a}}.$$

2.2 Linear-Elastic Facture Mechanics

Article IWB-3612 of Section XI [11] requires that the applied stress intensity factor, K_I, at the final flaw size be less than the available fracture toughness at the crack tip temperature, with appropriate safety factors, as outlined below.

Normal and upset conditions: $K_I < K_{Ia} / \sqrt{10}$

where K_{Ia} is the fracture toughness based on crack arrest.

Emergency and faulted conditions: $K_I < K_{Ic} / \sqrt{2}$

where K_{Ic} is the fracture toughness based on crack initiation.

2.3 Elastic-Plastic Facture Mechanics

Elastic-plastic fracture mechanics (EPFM) will be used as alternative acceptance criteria when the flaw related failure mechanism is unstable ductile tearing. This type of failure falls between rapid, non-ductile crack extension and plastic collapse. Linear-elastic fracture mechanics (LEFM) would be used to assess the potential for non-ductile failure, whereas limit load analysis would be used to check for plastic collapse.

2.3.1 Screening Criteria

Screening criteria for determining failure modes in ferritic materials may be found in Appendix H of Section XI. Although Appendix H, Article H-4200 [11] contains specific rules for evaluating flaws in Class 1 ferritic piping, its screening criteria may be adapted to other ferritic components, such as the reactor vessel head, as follows:

Let,

$$K_r' = K_{Iapp} / K_{Ic}$$
$$S_r' = \sigma_{max} / \sigma_f$$

Then the appropriate method of analysis is determined by the following limits:

LEFM Regime:	$K_r' / S_r' \geq 1.8$
EPFM Regime:	$1.8 > K_r' / S_r' \geq 0.2$
Limit Load Regime:	$0.2 > K_r' / S_r'$

2.3.2 Flaw Stability and Crack Driving Force

Elastic-plastic fracture mechanics analysis will be performed using a J-integral/tearing modulus (J-T) diagram to evaluate flaw stability under ductile tearing, where J is either the applied (J_{app}) or the material (J_{mat}) J-integral, and T is the tearing modulus, defined as $(E/\sigma_f^2)(dJ/da)$. The crack driving force, as measured by J_{app}, is also checked against the J-R curve at a crack extension of 0.1 inch ($J_{0.1}$). Consistent with industry practice for the evaluation of flaws in partial penetration welded nozzles,

different safety factors will be utilized for primary and secondary loads. Flaw stability assessments for normal and upset conditions will consider a safety factor of 3 on the stress intensity factor due to primary (pressure) stresses and a safety factor of 1.5 for secondary (residual plus thermal) stresses. The crack driving force will be calculated using safety factors of 1.5 and 1 for primary and secondary stresses, respectively. For EPFM analysis of faulted conditions, safety factors of 1.5 and 1 will be used for flaw stability assessments and 1.5 and 1 for evaluations of crack driving force.

The general methodology for performing an EPFM analysis is outlined below.

Let

$$E' = E/(1-\nu^2)$$

$$\text{Final flaw depth} = a$$

$$\text{Total applied } K_I = K_{Iapp}$$

$$K_I \text{ due to pressure (primary)} = K_{Ip} \text{ (from Appendix B)}$$

$$K_I \text{ due to residual plus thermal (secondary)} = K_{Is} = K_{Iapp} - K_{Ip}$$

$$\text{Safety factor on primary loads} = SF_p$$

$$\text{Safety factor on secondary loads} = SF_s$$

For small scale yielding at the crack tip, a plastic zone correction is used to calculate an effective flaw depth based on

$$a_e = a + [1/(6\pi)]\,[\,(K_{Ip} + K_{Is}) / \sigma_y\,]^2,$$

which is used to update the stress intensity factors based on

$$K'_{Ip} = K_{Ip}\sqrt{\frac{a_e}{a}}$$

and

$$K'_{Is} = K_{Is}\sqrt{\frac{a_e}{a}}.$$

The applied J-integral is then calculated using the relationship

$$J_{app} = (SF_p{*}K'_{Ip} + SF_s{*}K'_{Is})^2/E'.$$

The final parameter needed to construct the J-T diagram is the tearing modulus. The applied tearing modulus, T_{app}, is calculated by numerical differentiation for small increments of crack size (da) about the final crack size (a), according to

$$T_{app} = \frac{E}{\sigma_f^2}\left[\frac{J_{app}(a+da) - J_{app}(a-da)}{2(da)}\right].$$

Using the power law expression for the J-R curve,

$$J_{mat} = C(\Delta a)^m,$$

the material tearing modulus, T_{mat}, can be expressed as

$$T_{mat} = (E/\sigma_f^2)Cm(\Delta a)^{m-1}.$$

Constructing the J-T diagram,

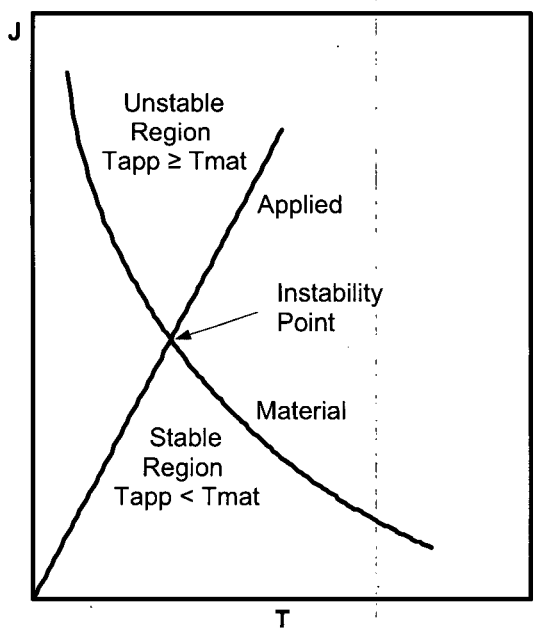

flaw stability is demonstrated at an applied J-integral when the applied tearing modulus is less than the material tearing modulus. Alternately, the applied J-integral is less than the J-integral at the point of instability.

To complete the EPFM analysis, it must be shown that the applied J-integral is less than $J_{0.1}$, demonstrating that the crack driving force falls below the J-R curve at a crack extension of 0.1 inch.

3.0 ASSUMPTIONS

This section discusses assumptions and modeling simplifications applicable to the present evaluation of the DB-1 CRDM nozzle remnant flaw.

3.1 Unverified Assumptions

There are no assumptions that must be verified before the present analysis can be used to support the CRDM nozzle IDTB repair at Davis Besse Unit 1.

3.2 Justified Assumptions

The size of the J-groove weld prep and the thickness of the buttering are based on nominal dimensions. This is considered to be standard practice in stress analysis and fracture mechanics analysis. It is conservatively assumed that the postulated flaw extends through the entire J-groove weld and butter.

3.3 Modeling Simplifications

The finite element computer models used to generate residual stresses and transient operational stresses do not include the ID temper bead repair weld. This is deemed to be an appropriate modeling simplification considering the very local effect of the repair weld on stresses in the J-groove weld.

4.0 DESIGN INPUTS

This section provides basic input data needed to perform a fatigue crack growth analysis and a flaw evaluation of the final flaw size.

4.1 Materials

4.1.1 Mechanical and Thermal Properties

Table 4-1, Table 4-2, and Table 4-3 list the temperature dependent values of modulus of elasticity (E), Poisson's ratio (ν), and coefficient of thermal expansion (α) properties used in the finite element crack models. These properties are obtained from a previous stress analysis model of the Davis Besse CRDM nozzle and reactor vessel head [8]. Mechanical properties for the low alloy steel head are also provided in Table 4-1, where the flow stress is the average of the yield and ultimate strengths. The yield and ultimate strength values are obtained from Supplemental Requirements for SA-533 Manganese-Molybdenum-Nickel Alloy Steel Plates in the 1968 original construction code [9].

Component	Material
RV head	SA-533 Grade B Class 1 [2]
Cladding	Stainless steel (use Type 316 properties)
J-groove weld filler	Alloy 182 [2] (use Alloy 600 properties for SB-167)
J-groove weld butter	Alloy 182 [2] (use Alloy 600 properties for SB-167)

Table 4-1: Material Properties for Head

Component	Head					
Material	SA-533 Grade B Class 1					
Temperature	E (10^6 psi)	ν	α (10^{-6} in./in./°F)	σ_y (ksi)	σ_u (ksi)	σ_f (ksi)
70	29.00	0.29	7.06	50.00	80.00	65.00
100	29.00	0.29	7.06	50.00	80.00	65.00
200	28.50	0.29	7.34	47.15	76.45	61.80
300	28.00	0.29	7.43	45.25	76.40	60.83
400	27.40	0.29	7.58	44.50	76.40	60.45
500	27.00	0.29	7.70	43.20	76.40	59.80
600	26.40	0.29	7.83	42.00	76.40	59.20
700	25.30	0.29	7.94	40.60	76.40	58.50

Table 4-2: Material Properties for Weld Metal

Component	Weld Butter and Weld Filler		
Material	Use Alloy 600 (SB-167)		
Temperature	E (10^6 psi)	ν	α (10^{-6} in./in./°F)
70	30.82	0.3	6.90
100	30.82	0.3	6.90
200	30.20	0.3	7.20
300	29.90	0.3	7.40
400	29.50	0.3	7.57
500	29.00	0.3	7.70
600	28.70	0.3	7.82
700	28.20	0.3	7.94

Table 4-3: Material Properties for Cladding

Component	Cladding		
Material	Use Type 316 (16Cr-12Ni-2Mo) Stainless Steel		
Temperature	E (10^6 psi)	ν	α (10^{-6} in./in./°F)
70	28.14	0.3	8.54
100	28.14	0.3	8.54
200	27.60	0.3	8.76
300	27.00	0.3	8.97
400	26.50	0.3	9.21
500	25.80	0.3	9.42
600	25.30	0.3	9.60
700	24.80	0.3	9.76

4.1.2 Reference Temperature

Based on a highest measured RT_{NDT} of { }, a value of { } °F will be used as a conservative estimate of the RT_{NDT} for the SA-533, Grade B, Class 1 low alloy steel head material.

4.1.3 Fracture Toughness

From Article A-4200 of Section XI [11], the lower bound K_{Ia} fracture toughness for crack arrest can be expressed as

$$K_{Ia} = 26.8 + 12.445 \exp [\, 0.0145\, (T - RT_{NDT}) \,],$$

where T is the crack tip temperature, RT_{NDT} is the reference nil-ductility temperature of the material, K_{Ia} is in units of ksi√in, and T and RT_{NDT} are in units of °F. In the present flaw evaluations, K_{Ia} is limited to a maximum value of 200 ksi√in (upper-shelf fracture toughness). Using the above equation with an RT_{NDT} of { } °F, K_{Ia} equals 200 ksi√in at a crack tip temperature of { } °F.

A higher measure of fracture toughness is provided by the K_{Ic} fracture toughness for crack initiation, approximated in Article A-4200 of Section XI [11] by

$$K_{Ic} = 33.2 + 20.734 \exp [\, 0.02\, (T - RT_{NDT}) \,].$$

4.1.4 J-integral Resistance Curve

The J-integral resistance (J-R) curve, needed for the EPFM method of analysis, is obtained from the following power law expression for nuclear reactor pressure vessel steels [12],

$$J_R = C(\Delta a)^m,$$

where the coefficient, C, and exponent, m, depend on the Charpy V-notch upper-shelf energy, CVN, and the flow stress, σ_o or σ_f, as shown in Figure 4-1 and Figure 4-2.

An estimated value of the Charpy V-notch upper-shelf energy is available from a generic study of plate materials used in B&W fabricated reactor vessels [13]. This statistical analysis of { } determined with a 95% confidence that at least 95% of the population exhibited upper-shelf energies exceeding a lower tolerance value of { } ft-lbs in the transverse (weak) direction.

Using the above referenced Charpy V-notch upper-shelf energy correlation for the J-integral resistance curve with a Charpy V-notch upper-shelf energy of { } ft-lbs, the coefficients of the power law are found to be:

C = { }

m = { }

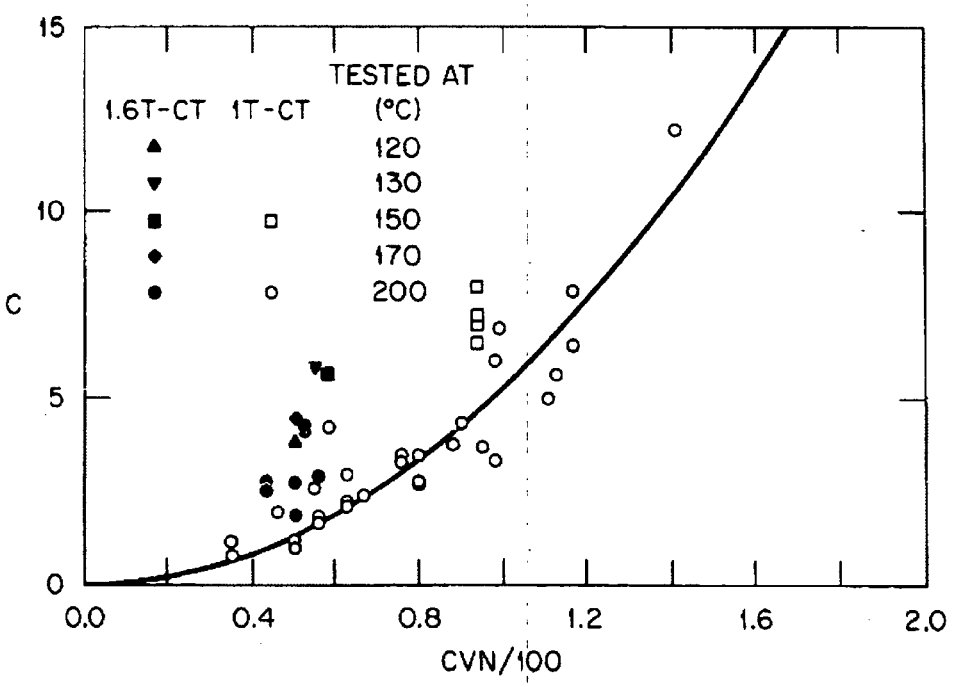

Figure 4-1: Correlation of Coefficient, C, of Power Law with Charpy V-Notch Upper Shelf Energy

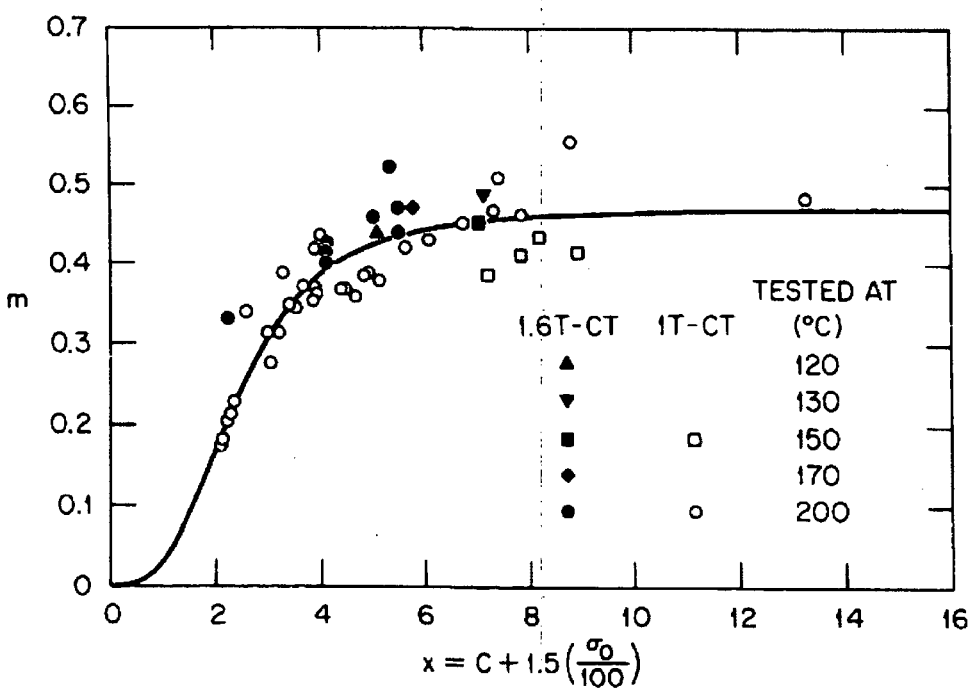

Figure 4-2: Correlation of Exponent, m, of Power Law with Coefficient, C, and Flow Stress, σ_o

4.1.5 Fatigue Crack Growth Rate

Flaw growth due to cyclic loading is calculated using the fatigue crack growth rate model from Article A-4300 of Section XI [11],

$$\frac{da}{dN} = C_o(\Delta K_I)^n,$$

where ΔK_I is the stress intensity factor range in ksi√in and da/dN is in inches/cycle. The crack growth rates for a surface flaw will be used for the evaluation of the corner crack since it is assumed that the degraded condition of the J-groove weld and butter exposes the low alloy steel head material to the primary water environment.

The following equations from Section XI [11] are used to model fatigue crack growth.

$$\Delta KI = KI_{max} - KI_{min}$$
$$R = KI_{min} / KI_{max}$$

$0 \le R \le 0.25$: $\Delta K_I < 17.74$,

$$n = 5.95$$
$$C_o = 1.02 \times 10^{-12} \times S$$
$$S = 1.0$$

$\Delta K_I \ge 17.74$,

$$n = 1.95$$
$$C_o = 1.01 \times 10^{-7} \times S$$
$$S = 1.0$$

$0.25 \le R \le 0.65$: $\Delta K_I < 17.74\,[\,(3.75R + 0.06) / (26.9R - 5.725)\,]^{0.25}$,

$$n = 5.95$$
$$C_o = 1.02 \times 10^{-12} \times S$$
$$S = 26.9R - 5.725$$

$\Delta K_I \ge 17.74\,[\,(3.75R + 0.06) / (26.9R - 5.725)\,]^{0.25}$,

$$n = 1.95$$
$$C_o = 1.01 \times 10^{-7} \times S$$
$$S = 3.75R + 0.06$$

$0.65 \le R < 1.0$: $\Delta K_I < 12.04$,

$$n = 5.95$$
$$C_o = 1.02 \times 10^{-12} \times S$$
$$S = 11.76$$

$\Delta K_I \ge 12.04$,

$$n = 1.95$$
$$C_o = 1.01 \times 10^{-7} \times S$$
$$S = 2.5$$

4.2 Basic Geometry

The reactor vessel head and original CRDM nozzle penetration are described by the following key dimensions:

Radius to base metal	= {	} in. [14]
Head thickness (minimum)	= {	} in. [14]
Cladding thickness (nominal)	= {	} in. [15]
Butter thickness (nominal)	= {	} in. [16] or { }
Penetration bore	= {	} in. [16]
Penetration angle at outermost nozzle	= {	} deg. [16]

Details of the CRDM nozzle penetration and J-groove weld are provided in the description of the finite element crack model in Appendix C.

4.3 Operating Transients

The most significant normal and upset condition transients for fatigue crack growth may be combined into a 'full-range' transient comprised of heatup to 100% power (HU), a Type B reactor trip (RT), and subsequent normal cooldown (CD). Full-range transients are associated with operating events that include a zero state of stress. The reactor coolant functional specification [17] provides pressure and temperature time-histories for these transients, and lists 240 design cycles for the heatup/cooldown transient and { } cycles for the Type B reactor trip.

The rod withdrawal accident (RWA) upset transient was also selected since it experiences a high reactor coolant pressure of { } psig. This is especially significant for EPFM flaw evaluations where primary pressure loads are subjected to higher safety factors than secondary thermal loads. Since it is not expected that a rod withdrawal accident will occur during a four year period of operation, the RWA transient is not included in the calculation of fatigue crack growth, but it is addressed when evaluating the acceptability of the final flaw size. Transient 11 of the functional specification represents this design transient as an in-surge to the pressurizer which is based on the event that results in the greatest RCS pressure and temperature change. This event is initiated from 15% power and results in a 550 psi increase in RCS pressure and a 15 °F increase in temperature. The transient is of short duration, lasting approximately 20 to 30 seconds, producing only a minimal increase in head temperature. The functional specification transient bounds the expected change in the RCS pressure and temperature from the same event if initiated from full power conditions. As provided in Figure 15.2.2-1 of the DB-1 UFSAR [18], a rod withdrawal event from full power results in an increase of only 30 psi and 1.5 °F.

The functional specification also specifies one emergency condition transient, a stuck open turbine bypass valve, and two faulted condition transients, a steam line break and a loss of coolant accident. Appendix F of the Section III stress analysis for the CRDM nozzle IDTB weld repair [19] concludes that the stresses resulting from the emergency and faulted condition transients are bounded by those for the reactor trip transient. And since the safety factors on fracture toughness are higher for normal/upset conditions than for emergency/faulted conditions (Table 1-1), and the K_{Ic} fracture toughness for crack initiation is higher than the K_{Ia} fracture toughness for crack arrest (Section 4.1.3), it follows that the present flaw evaluations for normal/upset conditions also serve as a bounding analysis for emergency

and faulted conditions. No further consideration of the emergency and faulted transients is therefore warranted.

4.4 Applied Stresses

Two sources of applied stress are considered for the present flaw evaluations, residual stresses from welding and stresses that occur during normal operation.

4.4.1 Residual Stresses

Residual stresses are obtained from a three-dimensional elastic-plastic finite element stress analysis performed by Dominion Engineering, Inc. [20]. Hoop stresses on the radial plane through the weld and butter are then mapped to the three-dimensional finite element crack model described in Section 2.1.1. Hoop stresses are used since these stresses are perpendicular to the crack face and therefore open the crack.

The DEI analysis simulated welding of the J-groove buttering, a post-weld heat treatment, welding of the J-groove partial penetration weld at the outmost CRDM nozzle, hydrostatic testing, operation at steady state temperature and pressure conditions, return to zero load conditions, removal of the original nozzle (Time 11006), and a second application of steady state loads. It is known from previous analysis that stresses at the outermost CRDM nozzle location conservatively bound stresses at all other nozzle locations [3]. The residual stresses in the remnant J-groove weld and butter are obtained from the load step corresponding to Time 11006, prior to the return to operating conditions

The DEI finite element model is shown in Figure 4-3, prior to removal of the CRDM nozzle. Figure 4-4 provides a closer view of the J-groove weld after the nozzle is removed.

4.4.2 Operational Stresses

Operational stresses are obtained by linear-elastic stress analysis using the three-dimensional finite element crack model described in Section 2.1.1, but with displacements normal to the crack face constrained to zero. Hoop stresses on a radial plane through the weld and butter are then copied directly to the crack model to facilitate the calculation of stress intensity factors along the entire crack front. Stresses are developed for the combined heatup/reactor trip/cooldown and rod withdrawal transients discussed in Section 4.3 using the thermal and structural finite element models described in Appendix D.

Figure 4-5 illustrates the "uncracked" finite element model used to calculate nodal temperatures (transient thermal analysis) and stresses (static stress analysis). The thermal phase of the solution is driven by wetted surface loads developed from time-dependent bulk fluid temperatures and convective heat transfer (film) coefficients. The structural model is then loaded by internal pressure (surface load) and nodal temperatures (body force loads from the thermal solution) to determine stresses at various times, as listed in Table 4-4. The critical time points are selected only after calculating stress intensity factors for each set of stresses output from the stress analysis solution. This process serves to maximize the stress intensity factors used in the fatigue crack growth analysis and the final flaw evaluations. The time points selected for use in the subsequent fracture mechanics analyses are identified in Table 4-4 by alphanumeric symbols.

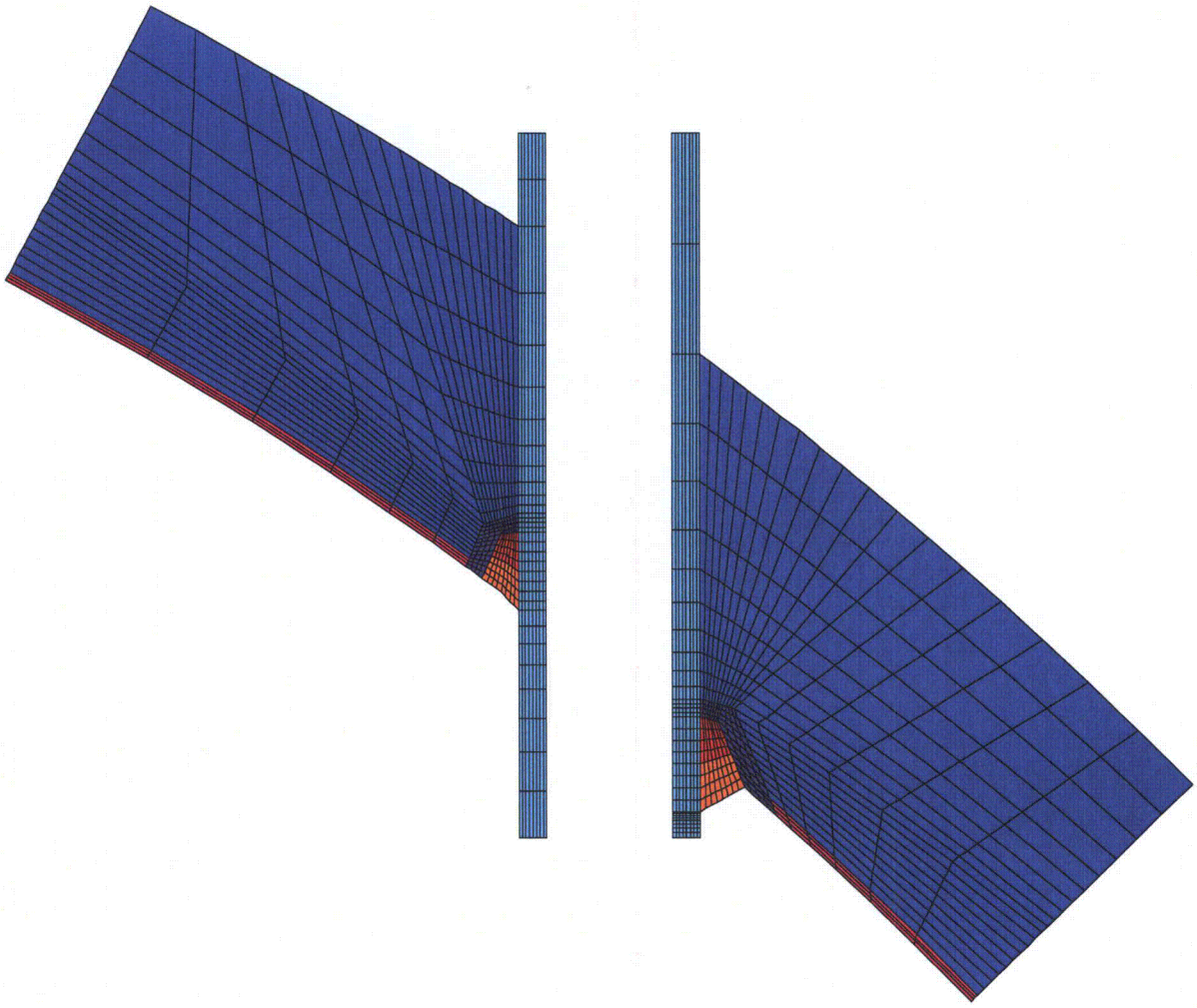

Figure 4-3: DEI Finite Element Stress Model

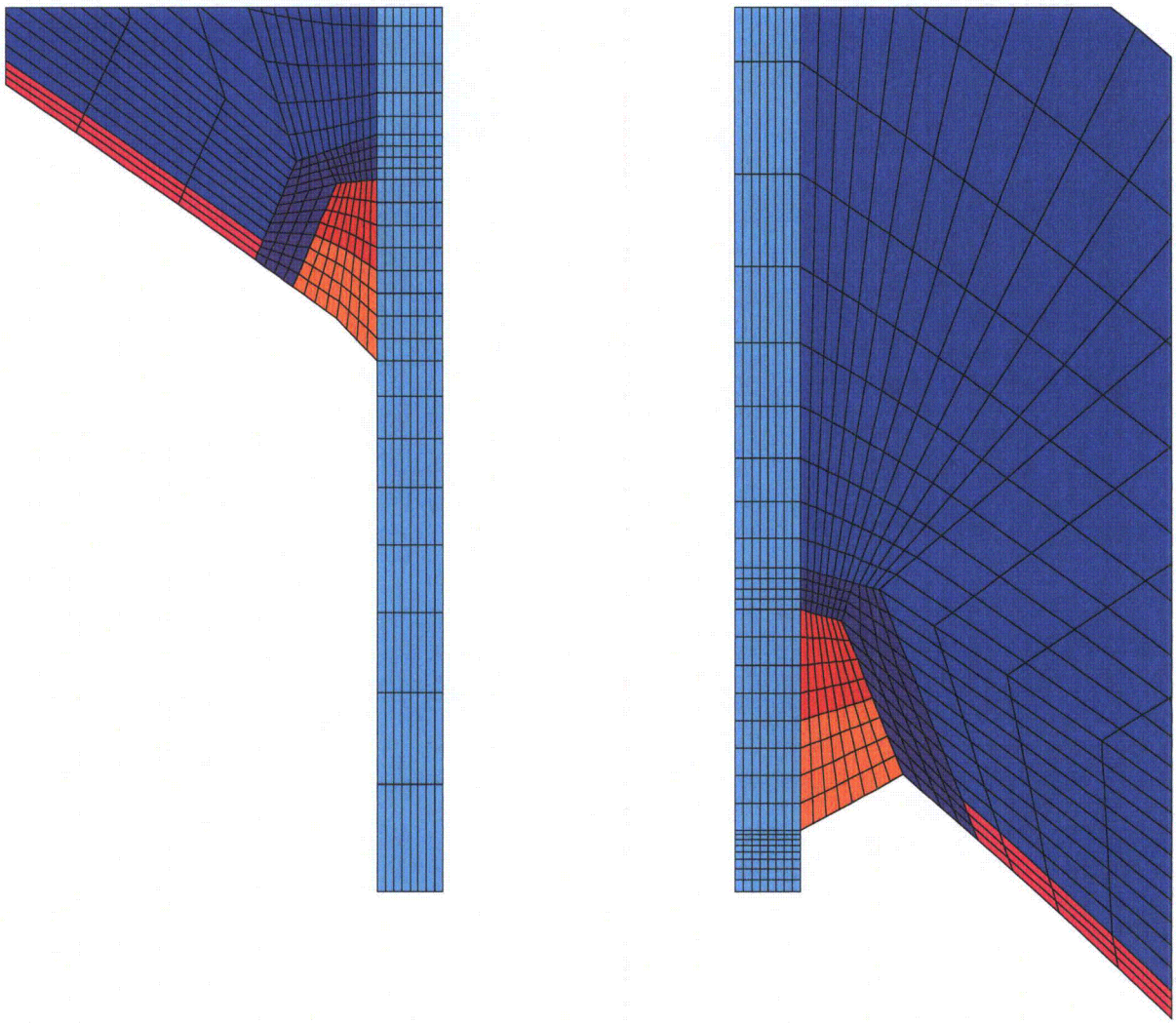

Figure 4-4: DEI Finite Element Stress Model – Weld Region

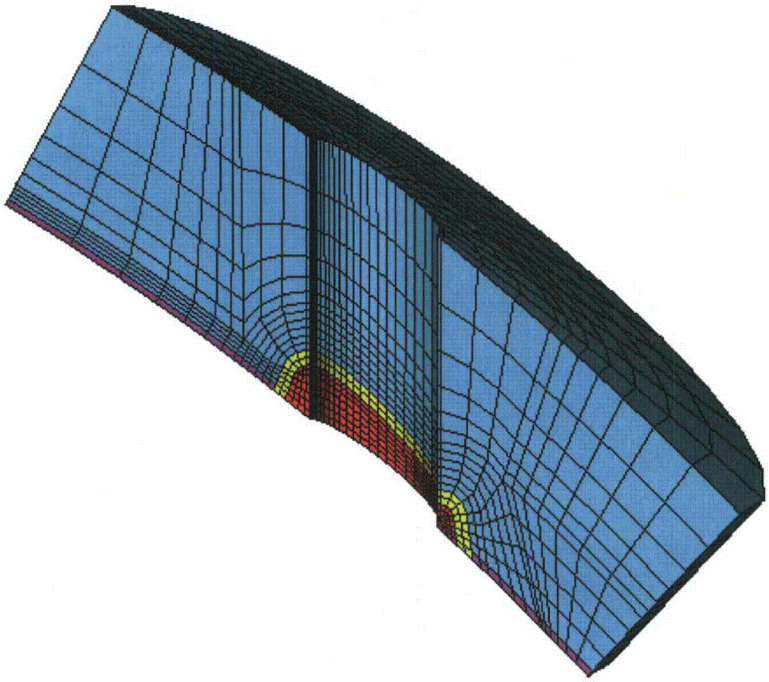

Figure 4-5: Finite Element Stress Model for Operational Stresses

Table 4-4: Transient Analysis Time Points for Operational Stresses

Symbol*	Load Step	Time (hours)	Temp. (F)	Pressure (psig)	Comment
Combined Heatup/Reactor Trip/Cooldown					
SD	1				Zero stress state
	2				End of heatup ramp
	3				After heatup ramp
	4				Steady state at 8% power
	5				End of power loading ramp (8%-100%)
	6				After power loading ramp (8%-100%)
SS	7				Steady state at 100% power
RT1	8				Reactor trip
	9				Reactor trip
RT2	10				Reactor trip
	11				End of cooldown ramp
Rod Withdrawal Accident					
	1				
RWA	2				Maximum pressure
	3				
	4				

*Symbols: SD = Shutdown
SS = Steady State
RT1 = Reactor Trip time 1
RT2 = Reactor Trip time 2
RWA = Rod Withdrawal Accident

5.0 CALCULATIONS

Propagation of a postulated initial flaw in the J-groove weld and butter is calculated to determine the final flaw size after a four year service interval. Flaw evaluations are then performed to assess the acceptability of the final flaw size.

5.1 Fatigue Crack Growth

Although it is believed that a PWSCC flaw would be confined to the J-groove weld and butter, it is postulated that a fatigue flaw would initiate in the low alloy steel head, combine with the PWSCC flaw, and propagate farther into the head under cyclic loads. Fatigue crack growth is calculated from stress intensity factors derived from a finite element crack model using residual stresses from a DEI stress analysis [20] and operational stresses calculated herein. The actual flaw growth calculations are presented in Table 5-1, along with a comparison of the final stress intensity factor with the LEFM acceptance criteria for each of the five significant load steps identified in Table 4-4. This table therefore serves several purposes; it determines the final flaw size at the end the designated service interval, it compares stress intensity factors at the final flaw size with LEFM acceptance criteria, and it serves as a means of identifying the controlling load steps for EPFM evaluation.

Crack growth is calculated for each heatup/cooldown cycle. Since the original design basis [17] specifies 240 heatup/cooldown cycles over a 40 year period, the corresponding time increment is one-sixth of a year.

Stress intensity factors are provided in Table 5-1 for all locations along the postulated crack front, including the cladding. It is apparent from the stress intensity factors listed in these tables for the initial flaw sizes that the highest value in the low alloy steel head occurs at the bored surface.

Table 5-1: Flaw Growth and LEFM Evaluation

INPUT DATA

Initial Flaw Size: Depth along bore, a_o = 2.035 in.

Fracture Toughness: Reference temperature of head, RTndt = { } F
Upper shelf toughness, UST = 200 ksi√in

KIc = 33.2 + 20.734 exp [0.02 (T - RTndt)] ≤ UST
KIa = 26.8 + 12.445 exp [0.0145 (T - RTndt)] ≤ UST

Stress Intensity Factors:

	Condition*	SD	SS	RT1	RT2	RWA	
	Temperature	70	608	610	530	600	F
	Pressure	0	2155	2450	1720	2745	psig
	Sy	50.0	41.9	41.9	42.8	42.0	ksi
	KIc	58.5	200.0	200.0	200.0	200.0	ksi√in
	KIa	41.2	200.0	200.0	200.0	200.0	ksi√in
	Crack Front	Stress Intensity Factor, KI					
	Position	(psi√in)	(psi√in)	(psi√in)	(psi√in)	(psi√in)	
Cladding Surface	1	72012	94317	99728	121749	113102	
	2	57085	80555	85683	103246	98142	
	3	51528	76707	81904	97080	94057	
	4	50744	77191	82454	95497	94199	
	5	51092	77988	83217	94302	94399	
	6	50355	76704	81732	90907	92098	
	7	50354	76451	81216	87459	90395	
	8	55409	84199	89223	94177	98404	
	9	58477	93779	99714	104872	110130	
Bored Surface	10	61779	101946	108634	114318	120167	

* Condition	Description
SD	Time step 1 at 0 hr. of heatup/reactor trip/cooldown (shutdown w/ only residual stress)
SS	Time step 7 at 10.000 hr. of heatup/reactor trip/cooldown (steady state at 100% power)
RT1	Time step 8 at 10.004 hr. of heatup/reactor trip/cooldown (during reactor trip)
RT2	Time step 10 at 10.141 hr. of heatup/reactor trip/cooldown (during reactor trip)
RWA	Time step 2 at 0.0044 hr. into rod withdrawal accident (high pressure condition)

Table 5-1: Flaw Growth and LEFM Evaluation (Cont'd)

FATIGUE CRACK GROWTH

Transient Description: 240 cycles over 40 years

ΔN = 6 cycles/year

			Crack Front Position 10						
Cycle	Operating Time (end of yr.)	a (in.)	RT2 KI(a)max (ksi√in)	SD KI(a)min (ksi√in)	ΔKI (ksi√in)	Δa (in.)	SS KI(a) (ksi√in)	RT1 KI(a) (ksi√in)	RWA KI(a) (ksi√in)
0	0.000	2.03500	114.318	61.779	52.539		101.946	108.634	120.167
1	0.167		114.398	61.822	52.576		102.018	108.710	120.252
2	0.333		114.479	61.866	52.613		102.089	108.787	120.336
3	0.500		114.559	61.909	52.650		102.161	108.863	120.421
4	0.667		114.640	61.953	52.687		102.233	108.940	120.505
5	0.833		114.720	61.997	52.724		102.305	109.016	120.590
6	1.000		114.801	62.040	52.761		102.377	109.093	120.675
7	1.167		114.882	62.084	52.798		102.449	109.170	120.760
8	1.333		114.963	62.127	52.835		102.521	109.247	120.845
9	1.500		115.043	62.171	52.872		102.593	109.323	120.930
10	1.667		115.124	62.215	52.910		102.665	109.400	121.015
11	1.833		115.205	62.258	52.947		102.737	109.477	121.100
12	2.000		115.286	62.302	52.984		102.809	109.554	121.185
13	2.167		115.367	62.346	53.021		102.882	109.631	121.270
14	2.333		115.448	62.390	53.059		102.954	109.708	121.355
15	2.500		115.530	62.434	53.096		103.026	109.785	121.441
16	2.667		115.611	62.478	53.133		103.099	109.862	121.526
17	2.833		115.692	62.522	53.170		103.171	109.940	121.611
18	3.000		115.773	62.565	53.208		103.244	110.017	121.697
19	3.167		115.855	62.609	53.245		103.316	110.094	121.782
20	3.333		115.936	62.653	53.283		103.389	110.172	121.868
21	3.500		116.018	62.697	53.320		103.462	110.249	121.953
22	3.667		116.099	62.742	53.358		103.534	110.327	122.039
23	3.833		116.181	62.786	53.395		103.607	110.404	122.125
24	4.000		116.262	62.830	53.433		103.680	110.482	122.211

Table 5-1: Flaw Growth and LEFM Evaluation (Cont'd)

LEFM FRACTURE TOUGHNESS MARGINS

Period of Operation: Time = 4 years

Flaw Size: a = { } in.

	Loading Conditions					
	SD	SS	RT1	RT2	RWA	
Fracture Toughness, KIc	58.5	200.0	200.0	200.0	200.0	ksi√in
Fracture Toughness, KIa	41.2	200.0	200.0	200.0	200.0	ksi√in
Position 10						
KI(a)	62.830	103.680	110.482	116.262	122.211	ksi√in
a_e	2.1886	2.4298	2.4744	2.4955	2.5540	in.
KI(a_e)	64.068	111.398	119.789	126.594	134.621	ksi√in
Margin = KIc / KI(a_e)	n/a	n/a	n/a	n/a	n/a	
Margin = KIa / KI(a_e)	0.64	1.80	1.67	1.58	1.49	

where: $ae = a + 1/(6\pi)\,[KI(a)/Sy]^2$

$KI(a_e) = KI(a)*\sqrt{(a_e/a)}$

5.2 LEFM Flaw Evaluations

The results of the linear-elastic fracture mechanics flaw evaluations are summarized below for the final size of the postulated flaw after fatigue crack growth.

Flaw Size

Initial flaw size, a_i = 2.035 in.

Final flaw size after 4 years, a_f = { } in.

Flaw growth, Δa = { } in.

Controlling Transients	Shutdown	Heatup/Cooldown w/ Reactor Trip (RT2)	Rod Withdrawal Accident
Condition	Low Temperature	Normal	Upset
Temperature,	T = 70 °F	{ } °F	{ } °F
Fracture toughness,	K_{Ia} = 41.2 ksi√in	200.0 ksi√in	200.0 ksi√in
Final stress intensity factor,	$K_I(a_f)$ = 62.8 ksi√in	116.3 ksi√in	122.2 ksi√in
Effective flaw size,	a_e = 2.189 in.	2.500 in.	2.554 in.
Effective stress intensity factor,	$K_I(a_e)$ = 64.1 ksi√in	126.6 ksi√in	134.6 ksi√in
Fracture toughness margin (> 3.16),	K_{Ia} / $K_I(a_e)$ = 0.64	1.58	1.49

Since the controlling fracture toughness margins are less than the Code required minimums, EPFM flaw evaluations will be performed to account for the ductile behavior of the low alloy steel during stable crack growth.

5.3 EPFM Flaw Evaluations

The elastic-plastic fracture mechanics procedure described in Section 2.3 is used to evaluate the final size of the postulated flaw after fatigue crack growth.

Flaw Size

Initial flaw size, a_i = 2.035 in.

Final flaw size after 4 years, a_f = { } in.

Controlling Transients	Shutdown	Heatup/Cooldown w/ Reactor Trip (RT2)	Rod Withdrawal Accident
SCREENING PROCEDURE			
	T = 70 °F	{ } °F	{ } °F
	E = 29000 ksi	26820 ksi	26400 ksi
	ν = 0.3	0.3	0.3
	$E' = E/(1-\nu^2)$ = 31860 ksi	29470 ksi	29010 ksi
	σ_y = 50.0 ksi	42.8 ksi	42.0 ksi
	σ_u = 80.0 ksi	76.4 ksi	76.4 ksi
	σ_f = 65.0 ksi	59.6 ksi	59.2 ksi
Crack initiation toughness,	K_{Ic} = 58.5 ksi√in	200.0 ksi√in	200.0 ksi√in
Total applied K_I,	$K_I(a_e)$ = 64.1 ksi√in	126.6 ksi√in	134.6 ksi√in
Then,	$K_r' = K_I(a_e) / K_{Ic}$ = 1.095	0.633	0.673

From finite element stress analysis, the maximum crack face stresses due to residual stress, pressure, and thermal gradients are

	σ'_{max} = 66.4 ksi	110.9 ksi	114.5 ksi
Then,	$S_r' = \sigma_{max} / \sigma_f$ = 1.022	1.860	1.934
Screening ratio,	K_r' / S_r' = 1.072	0.340	0.348

The analysis is therefore in the EPFM regime ($1.8 > K_r' / S_r' \geq 0.2$) for both loading conditions.

EPFM ANALYSIS

Total applied K_I,	$K_I(a)$ = 62.8 ksi√in	116.3 ksi√in	122.2 ksi√in
K_I primary (pressure from Appendix E),	$K_{Ip}(a)$ = 0.0 ksi√in	39.8 ksi√in	63.6 ksi√in
K_I secondary (residual plus thermal),	$K_{Is}(a)$ = 62.8 ksi√in	76.4 ksi√in	58.6 ksi√in
Multiplying by $\sqrt{(a_e/a)}$,	$K'_{Ip}(a)$ = 0.0 ksi√in	43.4 ksi√in	70.1 ksi√in
	$K'_{Is}(a)$ = 64.1 ksi√in	83.2 ksi√in	64.6 ksi√in

Table 5-2, Table 5-3, and Table 5-4 develop all the data necessary to construct J-T diagrams for the controlling operating conditions. The J-T diagrams are presented in Figure 5-1, Figure 5-2, and Figure 5-3.

For shutdown conditions, Table 5-2 shows for an applied J-integral of 0.290 kips/in, corresponding to safety factors of 3 and 1.5, the applied tearing modulus, 0.945, is less than the material tearing modulus, 318.0, indicating flaw stability. Alternately, the applied J-integral is less than the J-integral, 3.411 kips/in, at the point of instability. For safety factors of 1.5 and 1, the applied J-integral of 0.129 kips/in is less than the $J_{0.1}$ value of 1.350 kips/in, demonstrating that the crack driving force falls below the J-R curve at a crack extension of 0.1 inch.

For the heatup/cooldown transient with reactor trip, Table 5-3 shows for an applied J-integral of 2.206 kips/in, corresponding to safety factors of 3 and 1.5, the applied tearing modulus, 7.908, is less than the material tearing modulus, 22.15, indicating flaw stability. Alternately, the applied J-integral is less than the J-integral, 3.398 kips/in, at the point of instability. For safety factors of 1.5 and 1, the applied J-integral of 0.746 kips/in is less than the $J_{0.1}$ value of 1.363 kips/in, demonstrating that the crack driving force falls below the J-R curve at a crack extension of 0.1 inch.

For rod withdrawal accident conditions, Table 5-4 shows for an applied J-integral of 3.249 kips/in, corresponding to safety factors of 3 and 1.5, the applied tearing modulus, 11.63, is less than the material tearing modulus, 12.93, indicating flaw stability. Alternately, the applied J-integral is less than the J-integral, 3.397 kips/in, at the point of instability. For safety factors of 1.5 and 1, the applied J-integral of 0.992 kips/in is less than the $J_{0.1}$ value of 1.364 kips/in, demonstrating that the crack driving force falls below the J-R curve at a crack extension of 0.1 inch.

Table 5-2: EPFM Evaluation for Shutdown Conditions

EPFM Equations:

$J_{mat} = C(\Delta a)^m$ $\quad C = \{ \quad \}$

$T_{mat} = (E/\sigma_f^2)*Cm(\Delta a)^{m-1}$ $\quad m = \{ \quad \}$

$J_{app} = (SF_p*K'_{Ip}+SF_s*K'_{Is})^2/E'$

$T_{app} = (E/\sigma_f^2)*(dJ_{app}/da)$

Ductile Crack Growth Stability Criterion: $T_{app} < T_{mat}$

At instability: $T_{app} = T_{mat}$

Safety Factors		$SF*K'_{Ip}$	$SF*K'_{Is}$	J_{app}	T_{app}	Stable?
Primary	Secondary	(ksi√in)	(ksi√in)	(kips/in)		
1.00	1.00	0.000	64.068	0.129	0.420	Yes
2.00	2.00	0.000	128.136	0.515	1.681	Yes
3.00	1.50	0.000	96.102	0.290	0.945	Yes
5.00	5.00	0.000	320.339	3.221	10.503	Yes
7.00	7.00	0.000	448.475	6.313	20.587	No

Iterate on safety factor until $T_{app} = T_{mat}$ to determine $J_{instability}$:

				$J_{instability}$	T_{app}	T_{mat}
5.1454	5.1454	0.000	329.655	3.411	11.123	11.123

at J_{mat} = 0.290 kips/in, T_{mat} = 317.951

Applied J-Integral Criterion: $J_{app} < J_{0.1}$

where, $J_{0.1} = J_{mat}$ at $\Delta a = 0.1$ in.

Safety Factors		$SF*K'_{Ip}$	$SF*K'_{Is}$	J_{app}	$J_{0.1}$	OK?
Primary	Secondary	(ksi√in)	(ksi√in)	(kips/in)	(kips/in)	
1.50	1.00	0.000	64.068	0.129	1.350	Yes

Table 5-3: EPFM Evaluation for Heatup/Cooldown with Reactor Trip

EPFM Equations:

$J_{mat} = C(\Delta a)^m$ $\quad C = \{ \quad \}$

$T_{mat} = (E/\sigma_f^2)*Cm(\Delta a)^{m-1}$ $\quad m = \{ \quad \}$

$J_{app} = (SF_p*K'_{Ip}+SF_s*K'_{Is})^2/E'$

$T_{app} = (E/\sigma_f^2)*(dJ_{app}/da)$

Ductile Crack Growth Stability Criterion: $T_{app} < T_{mat}$

At instability: $T_{app} = T_{mat}$

Safety Factors		$SF*K'_{Ip}$	$SF*K'_{Is}$	J_{app}	T_{app}	Stable?
Primary	Secondary	(ksi√in)	(ksi√in)	(kips/in)		
1.00	1.00	43.391	83.204	0.544	1.949	Yes
2.00	1.00	86.782	83.204	0.980	3.515	Yes
3.00	1.50	130.172	124.806	2.206	7.908	Yes
5.00	1.00	216.954	83.204	3.057	10.959	Yes
7.00	1.00	303.736	83.204	5.080	18.212	No

Iterate on safety factor until $T_{app} = T_{mat}$ to determine $J_{instability}$:

				$J_{instability}$	T_{app}	T_{mat}
2.4998	2.4998	108.468	207.992	3.398	12.182	12.182

at J_{mat} = 2.206 kips/in, T_{mat} = 22.150

Applied J-Integral Criterion: $J_{app} < J_{0.1}$

where, $J_{0.1} = J_{mat}$ at $\Delta a = 0.1$ in.

Safety Factors		$SF*K'_{Ip}$	$SF*K'_{Is}$	J_{app}	$J_{0.1}$	OK?
Primary	Secondary	(ksi√in)	(ksi√in)	(kips/in)	(kips/in)	
1.50	1.00	65.086	83.204	0.746	1.363	Yes

Table 5-4: EPFM Evaluation for Rod Withdrawal Accident

EPFM Equations:

$J_{mat} = C(\Delta a)^m$ $\quad C = \{ \quad \}$

$T_{mat} = (E/\sigma_f^2)*Cm(\Delta a)^{m-1}$ $\quad m = \{ \quad \}$

$J_{app} = (SF_p*K'_{Ip}+SF_s*K'_{Is})^2/E'$

$T_{app} = (E/\sigma_f^2)*(dJ_{app}/da)$

Ductile Crack Growth Stability Criterion: $T_{app} < T_{mat}$

At instability: $T_{app} = T_{mat}$

Safety Factors		$SF*K'_{Ip}$	$SF*K'_{Is}$	J_{app}	T_{app}	Stable?
Primary	Secondary	(ksi√in)	(ksi√in)	(kips/in)		
1.00	1.00	70.055	64.566	0.625	2.236	Yes
2.00	1.00	140.110	64.566	1.444	5.168	Yes
3.00	1.50	210.165	96.849	3.249	11.628	Yes
5.00	1.00	350.275	64.566	5.932	21.231	No
7.00	1.00	490.384	64.566	10.616	37.993	No

Iterate on safety factor until $T_{app} = T_{mat}$ to determine $J_{instability}$:

				$J_{instability}$	T_{app}	T_{mat}
2.3320	2.3320	163.367	150.567	3.397	12.158	12.158

at J_{mat} = 3.249 kips/in, T_{mat} = 12.933

Applied J-Integral Criterion: $J_{app} < J_{0.1}$

where, $J_{0.1} = J_{mat}$ at $\Delta a = 0.1$ in.

Safety Factors		$SF*K'_{Ip}$	$SF*K'_{Is}$	J_{app}	$J_{0.1}$	OK?
Primary	Secondary	(ksi√in)	(ksi√in)	(kips/in)	(kips/in)	
1.50	1.00	105.082	64.566	0.992	1.364	Yes

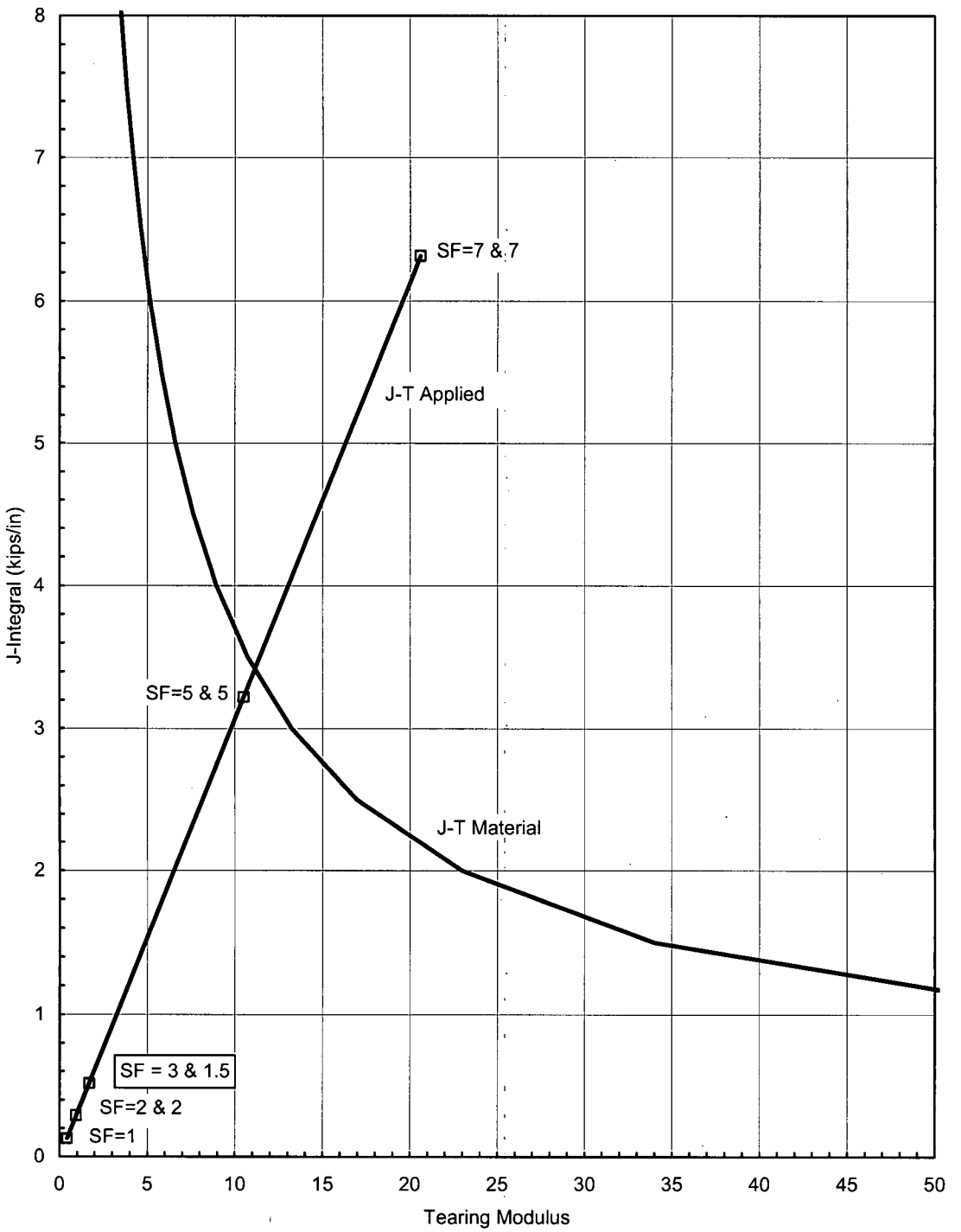

Figure 5-1: J-T Diagram for Shutdown Conditions

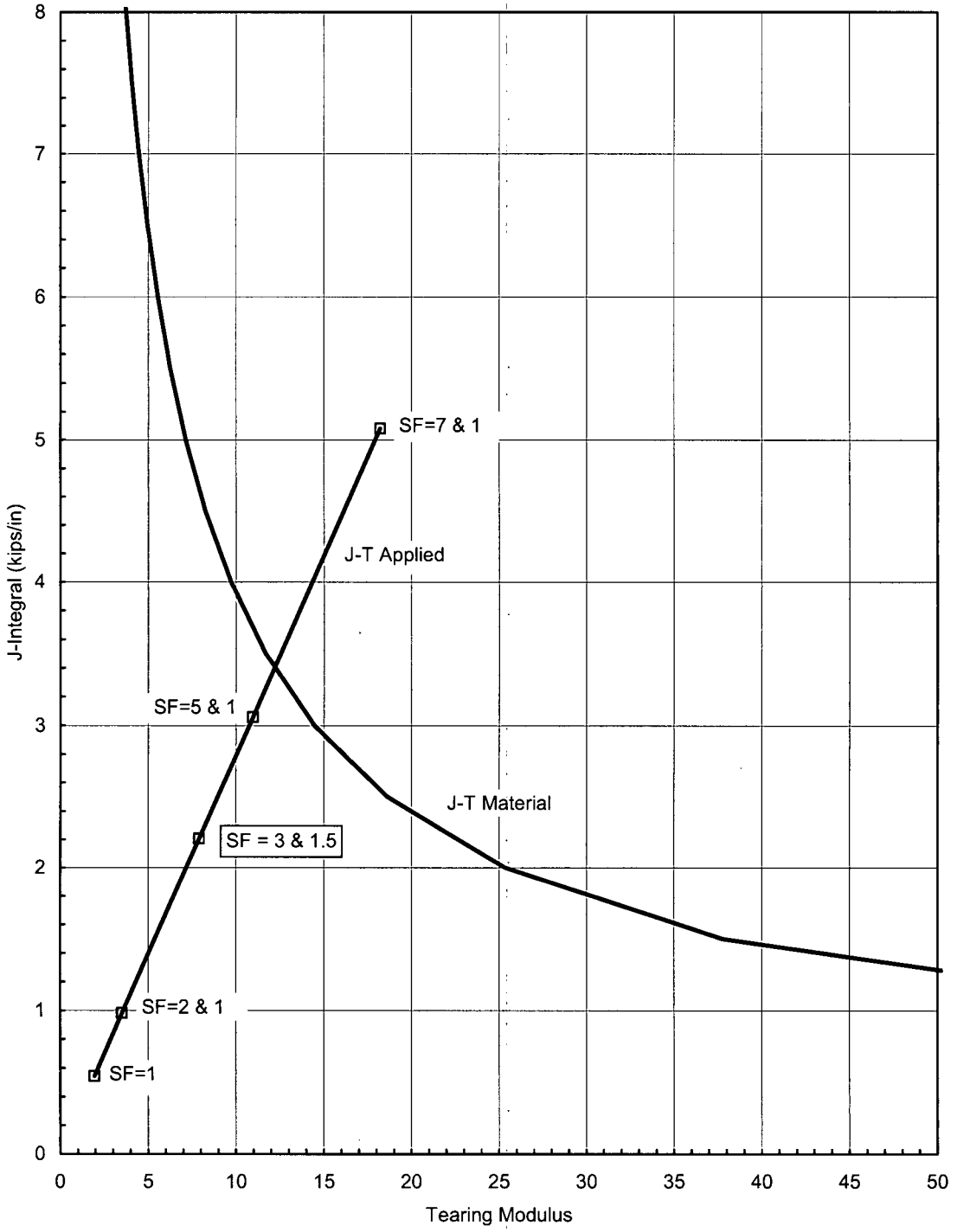

Figure 5-2: J-T Diagram for Heatup/Cooldown with Reactor Trip

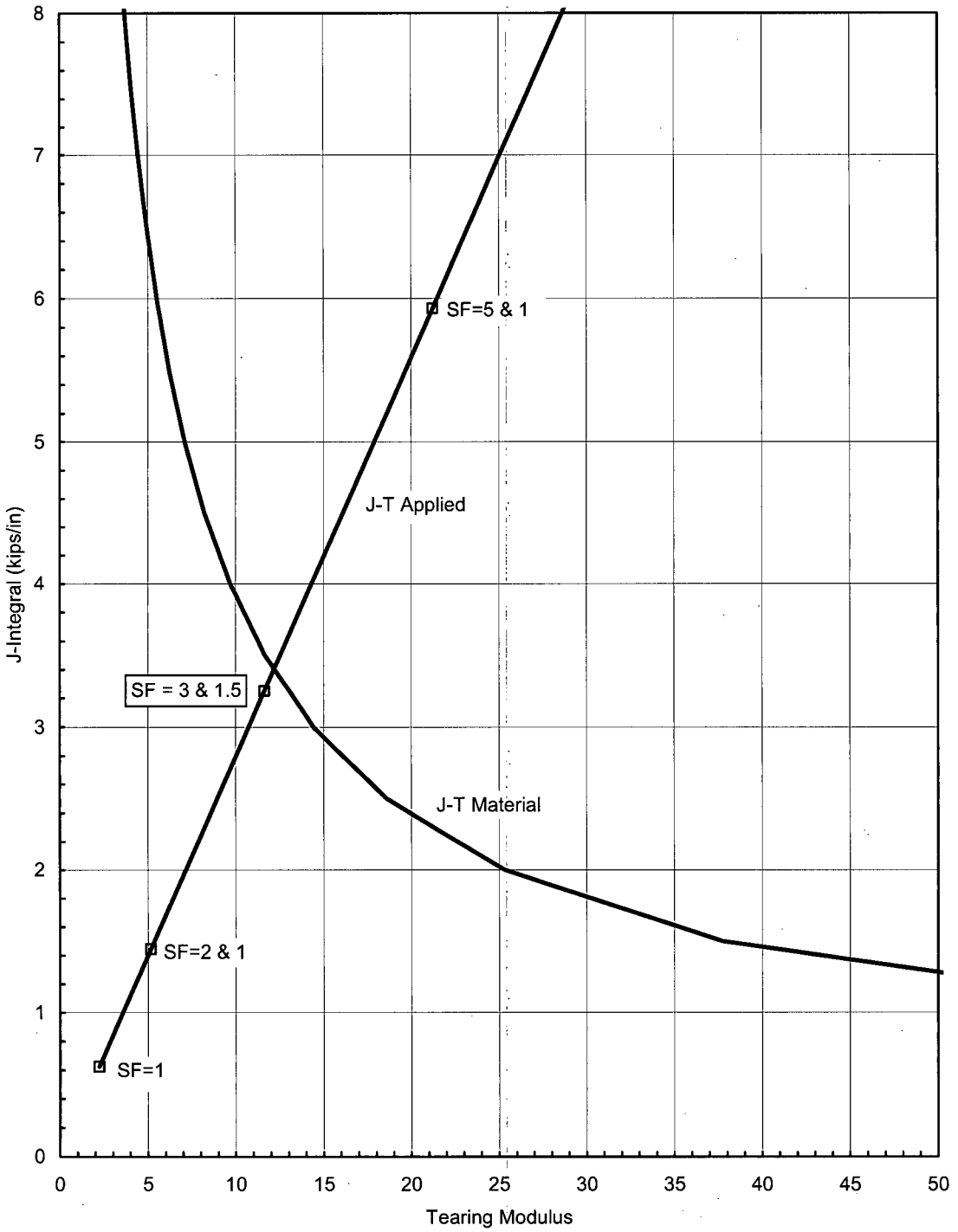

Figure 5-3: J-T Diagram for Rod Withdrawal Accident

6.0 SUMMARY OF RESULTS AND CONCLUSIONS

Elastic-plastic fracture mechanics has been used to evaluate a postulated radial flaw in the J-groove weld and butter of an outermost CRDM nozzle reactor vessel head penetration. The final flaw size was determined by linear elastic fracture mechanics for 4 years of fatigue crack growth.

6.1 Summary of Results

Flaw Size

Initial flaw size, a_i = 2.035 in.

Final flaw size after 4 years, a_f = { } in.

Controlling Transients	Shutdown	Heatup/Cooldown w/ Reactor Trip	Rod Withdrawal Accident
Temperature,	T = 70 °F	{ } °F	{ } °F
Safety factors (primary/secondary),	SF = 3 / 1.5	3 / 1.5	3 / 1.5
Material tearing modulus,	T_{mat} = 318.0	22.15	12.93
Applied tearing modulus (< T_{mat})	T_{app} = 0.945	7.908	11.63
Safety factors (primary/secondary),	SF = 1.5 / 1	1.5 / 1	1.5 / 1
Material J-integral,	$J_{0.1}$ = 1.350 kips/in	1.363 kips/in	1.364 kips/in
Applied J-integral (< $J_{0.1}$)	J_{app} = 0.129 kips/in	0.746 kips/in	0.992 kips/in

6.2 Conclusion

Based on a combination of linear elastic and elastic plastic fracture mechanics analysis of a postulated remaining flaw in the original Alloy 182 J-groove weld and butter material, a Davis Besse Unit 1 CRDM nozzle is considered to be acceptable for at least 4 years of operation following an IDTB weld repair.

7.0 REFERENCES

1. AREVA NP Drawing 02-9134305-002, "Davis Besse CRDM Nozzle ID Temper Bead Weld Repair."

2. AREVA NP Document 08-9134304-000, "Davis Besse RVCH CRDM Penetration Modification," March 2010.

3. AREVA NP Document 38-1288564-00, "Calculation Number C-3206-00-1, Rev. 0, Davis Besse CRDM Stress Analysis," December 2001.

4. AREVA NP Document 51-5012047-00, "Stress Corrosion Cracking of Low Alloy Steel," March 2001.

5. AREVA NP Document 32-9066059-000, "Watts Bar CRDM Nozzle IDTB J-Groove Weld Analysis," December 2007.

6. ANSYS Finite Element Computer Code, Version 10.0, ANSYS Inc., Canonsburg, PA.

7. T.L. Anderson, Fracture Mechanics: Fundamentals and Applications, CRC Press, 1991.

8. AREVA NP Document 32-5011864-07, "CRDMH Connection 3D FE Model," March 2001.

9. ASME Boiler and Pressure Vessel Code, Section II, Material Specifications: Part A - Ferrous, 1965 Edition with Summer 1968 Addendum.

10. BAW-10046A, Rev. 2, "Methods of Compliance With Fracture Toughness and Operational Requirements of 10 CFR 50, Appendix G," B&W Owners Group Materials Committee Topical Report, June 1986.

11. ASME Boiler and Pressure Vessel Code, Section XI, Rules for Inservice Inspection of Nuclear Power Plant Components, 1995 Edition with Addenda through 1996.

12. NUREG-0744, Vol. 2, Rev. 1, "Resolution of the Task A-11 Reactor Vessel Materials Toughness Safety Issue," Appendix D, Materials Toughness Properties, Division of Safety Technology, Office of Nuclear Reactor Regulation, U.S. Nuclear Regulatory Commission, Washington, D.C. 20555, October 1982.

13. AREVA NP Document 77-2313-006 (BAW-2313, Revision 6), "B&W Fabricated Reactor Vessel Materials and Surveillance Data Information," AREVA NP Inc., November 2008.

14. AREVA NP Drawing 02-142178E-05, "Closure Head Center Disc." (DB-1 Midland Head)

15. AREVA NP Drawing 02-154613E-08, "Arrangement Reactor Vessel Longitudinal Section." (DB-1 Midland Head)

16. AREVA NP Drawing 02-142179E-10, "Closure Head Sub-Assembly." (DB-1 Midland Head)

17. AREVA NP Document 18-1149327-003, "Functional Specification for Reactor Coolant System for Davis-Besse," July 2008.

18. * Davis-Besse Nuclear Power Station No. 1 Updated Safety Analysis Report, Revision 26, June 2008.

19. AREVA NP Document 32-5012424-12, "CRDM Temper Bead Bore Weld Analysis," April 2004.

20. AREVA NP Document 32-9134665-000, "DEI Residual Stress Analysis for DB-1 CRDM Nozzle IDTB Repair," DEI Calc. No. C-8616-00-01, Rev. 0, Davis Besse CRDM Nozzle Welding Residual Stress Analysis, April 2010.

* Reference 18 is not retrievable from the AREVA NP Records Management system but are referenced here in accordance with AREVA NP Procedure 0402-01, Attachment 8. This customer reference is a valid source of design input as authorized by the Project Manager signature on page 2.

APPENDIX A: VERIFICATION OF COMPUTER CODE ANSYS

The ANSYS finite element computer program [6] is verified for use in the present flaw evaluation by executing three test cases from the ANSYS set of verification problems that utilize the SOLID90 thermal and SOLID95 structural 20-node 3-D solid elements. Test case VM161 determines heat flow in an insulated pipe. Test case VM148 analyzes a cantilevered, parabolic beam subjected to a static bending load. Test case VM143 calculates a stress intensity factor for a crack in a plate. All three test cases executed properly, as demonstrated below.

Verification Problem VM161

Thermal Analysis of an Insulated Pipe

File: vm161.vrt

VM161 RESULTS COMPARISON

Surface Heat Flow Rate

	TARGET	ANSYS	RATIO
q (BTU/hr)	362.0	362.0	1.000

Verification Problem VM148

Bending of a Parabolic Beam

File: vm148.vrt

VM148 RESULTS COMPARISON

End Displacement

	TARGET	ANSYS	RATIO
Y Deflection (in.)	-0.01067	-0.01062	0.995

Verification Problem VM143

Fracture Mechanics Analysis of a Crack in a Plate

File: vm143.vrt

VM143 RESULTS COMPARISON

Stress Intensity Factor by Displacement Extrapolation

	TARGET	ANSYS	RATIO
3-D ANALYSIS	1.0249	1.0620	1.036

APPENDIX B: COMPUTER FILES IN COLDSTOR

The computer files listed below, which remain unchanged from those listed in document 32-9134664-000, are stored in the AREVA NP COLDStor repository in the directory "\cold\41304\32-9134664-000\official".

ANSYS Models

File Name	Description	Modified Date	Installed Date
Uphill_Crack_Model.db	Crack model for uphill J-groove weld	03-19-10	04-12-10
Uphill_UnCrack_Model.db	Model for calculating operating stresses	03-20-10	04-12-10
MatlAndMesh.dat	Material data for thermal and stress analysis	04-04-10	04-12-10

ANSYS Thermal Analysis

File Name	Description	Modified Date	Installed Date
HU_RX8B_Thermal.dat	Input file for HU/RT/CD thermal analysis	04-04-10	04-12-10
HU_RX8B_Thermal.out	Output file for HU/RT/CD thermal analysis	04-05-10	04-12-10
RWA_Thermal.dat	Input file for RWA thermal analysis	04-04-10	04-12-10
RWA_Thermal.out	Output file for RWA thermal analysis	04-05-10	04-12-10

ANSYS Stress Analysis

File Name	Description	Modified Date	Installed Date
HU_RX8B_Stress.dat	Input file for HU/RT/CD stress analysis	04-04-10	04-12-10
HU_RX8B_Stress.out	Output file for HU/RT/CD stress analysis	04-04-10	04-12-10
RWA_Stress.dat	Input file for RWA stress analysis	04-04-10	04-12-10
RWA_Stress.out	Output file for RWA stress analysis	04-05-10	04-12-10

ANSYS Macros for Transferring Stresses to Crack Model

File Name	Description	Modified Date	Installed Date
Format_Stresses_Driver.mac	Driver to get residual stresses	03-28-10	04-12-10
Format_Stresses.mac	Macro to get residual stresses	03-28-10	04-12-10

File Name	Description	Modified Date	Installed Date
Get_Stresses_Driver.mac	Driver to get operating stresses	04-05-10	04-12-10
Get_Stresses.mac	Macro to get operating stresses	04-05-10	04-12-10

ANSYS Analysis to Calculate Stress Intensity Factors (SIF)

File Name	Description	Modified Date	Installed Date
Uphill_Crack_Pressure.inp	Input file for pressure loading	03-23-10	04-12-10
Press_Up.output	Output file for pressure loading	04-07-10	04-12-10
Get_RESI_SIFs.mac	Macro to get SIFs for residual stresses	04-08-10	04-12-10
Get_HUCD_SIFs.mac	Macro to get SIFs for HU/RT/CD stresses	04-05-10	04-12-10
Get_RWA_SIFs.mac	Macro to get SIFs for RWA stresses	04-05-10	04-12-10
Map_Stresses_Up.mac	Macro to map stresses from uncracked model to crack model	03-24-10	04-12-10
PrtKIup.mac	Macro to write SIFs to output file	03-24-10	04-12-10
RESIu.output	Output file for residual SIFs	04-08-10	04-12-10
HUCDu1.output	Output file for HU/RT/CD SIFs (load step 1)	04-05-10	04-12-10
HUCDu2.output	Output file for HU/RT/CD SIFs (load step 2)	04-05-10	04-12-10
HUCDu3.output	Output file for HU/RT/CD SIFs (load step 3)	04-05-10	04-12-10
HUCDu4.output	Output file for HU/RT/CD SIFs (load step 4)	04-05-10	04-12-10
HUCDu5.output	Output file for HU/RT/CD SIFs (load step 5)	04-05-10	04-12-10
HUCDu6.output	Output file for HU/RT/CD SIFs (load step 6)	04-05-10	04-12-10
HUCDu7.output	Output file for HU/RT/CD SIFs (load step 7)	04-05-10	04-12-10
HUCDu8.output	Output file for HU/RT/CD SIFs (load step 8)	04-05-10	04-12-10
HUCDu9.output	Output file for HU/RT/CD SIFs (load step 9)	04-05-10	04-12-10
HUCDu10.output	Output file for HU/RT/CD SIFs (load step 10)	04-05-10	04-12-10
HUCDu11.output	Output file for HU/RT/CD SIFs (load step 11)	04-05-10	04-12-10
RWAu1.output	Output file for RWA SIFs (load step 1)	04-05-10	04-12-10
RWAu2.output	Output file for RWA SIFs (load step 2)	04-05-10	04-12-10
RWAu3.output	Output file for RWA SIFs (load step 3)	04-05-10	04-12-10
RWAu4.output	Output file for RWA SIFs (load step 4)	04-05-10	04-12-10

ANSYS Verification

File Name	Description	Modified Date	Installed Date
vm161.vrt	Verification problem for thermal analysis	04-07-10	04-12-10
vm148.vrt	Verification problem for stress analysis	04-07-10	04-12-10
vm143.vrt	Verification problem for stress intensity factor	04-07-10	04-12-10

APPENDIX C: FINITE ELEMENT CRACK MODEL

C.1 Introduction

A non-radial partial penetration nozzle in a spherically shaped pressure vessel presents a challenging set of geometric constraints for both stress analysis and fracture mechanics analysis of flaws, especially in the J-groove weld. Since there are no closed-form solutions available to calculate stress intensity factors for such flaws, a three-dimensional finite element crack model is developed in this appendix for use in evaluating "J-shaped" flaws in the area of the partial penetration attachment weld.

The three-dimensional finite element model is constructed using crack tip elements along the entire J-shaped crack front, extending from the inside surface of the cladding to the bored surface of the penetration. An uncracked model of the nozzle, J-groove weld and butter, and a portion of the reactor vessel head and cladding is first created using the ANSYS finite element computer program [6]. After removing a block of elements around the crack front and inserting a sub-model of crack tip elements, stress intensity factors can be obtained via the program's KCALC routine. The crack tip sub-model consists of 20-node isoparametric elements that are collapsed to form wedges, with the appropriate mid-side nodes shifted to quarter-point locations to create a $1/\sqrt{r}$ singularity in strain at the crack tip.

C.2 Base Finite Element Model

A three-dimensional finite element model is constructed to represent an uncracked non-radial nozzle penetration in a hemi-spherical shaped head. This model utilizes the ANSYS SOLID95 3-D 20-node structural solid element, exclusively, so that a portion of the model can be readily removed and replaced with a crack tip sub-model.

C.2.1 Geometry

As shown in Figure C-1, the model is a 180-degree segment of the head, cladding, weld butter, and J-groove weld.

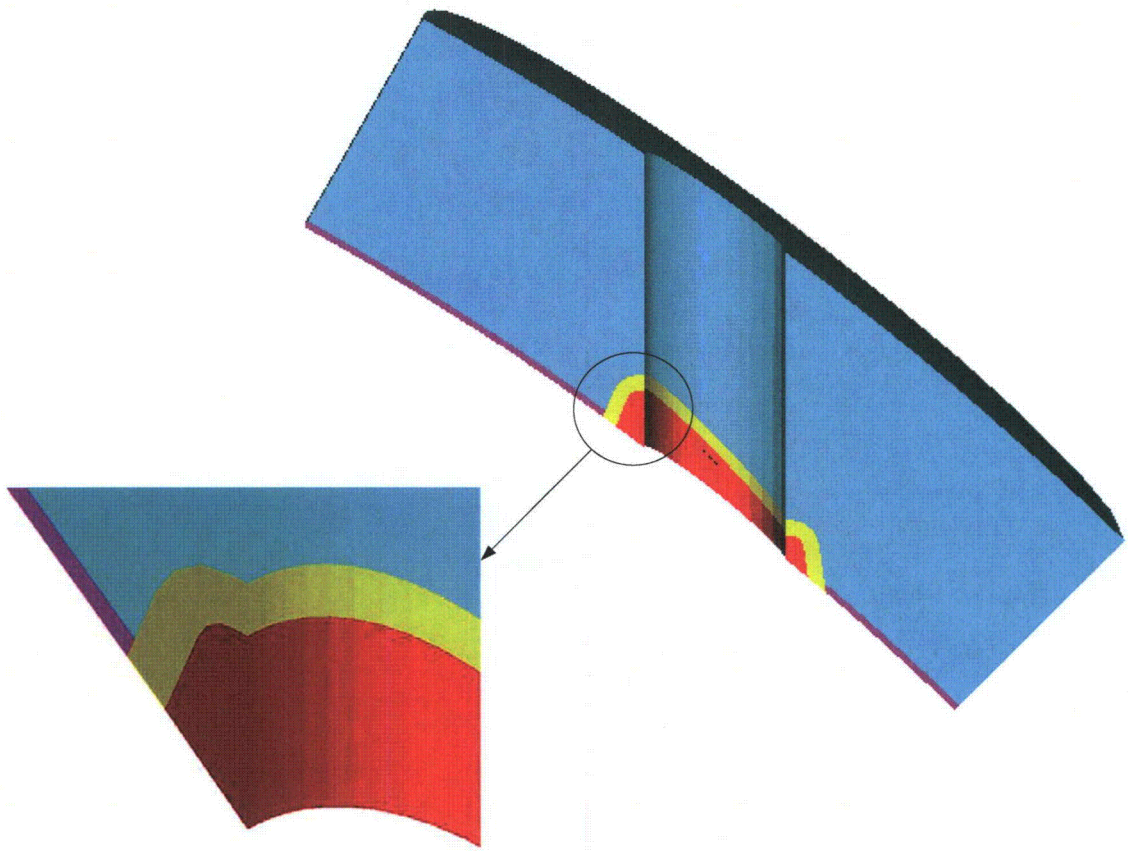

Figure C-1: Overall Model of Reactor Vessel Head Penetration

Key dimensions are:

Radius to base metal	= { } in. [14]
Head thickness (minimum)	= { } in. [14]
Cladding thickness (nominal)	= { } in. [15]
Butter thickness (nominal)	= { } in. [16] or { }
Hole diameter (original)	= { } in. [16] (near { } after machining [1])
J-groove weld center diameter	= { } in. [16]
J-groove weld angle	= { } deg. [16]
Basic J-groove radius	= { } in. [16]
Basic J-groove height	= { } in. [16] { }"
Additional height to base metal (nom.)	= { } in. [16] or { }
Horizontal distance to outermost nozzle	= { } in. [16]
Penetration angle at outermost nozzle	= { } deg.

C.2.2 Materials

The material designations of the various components of the model are:

Component	Material
RV head	SA-533 Grade B Class 1 [2]
Cladding	Stainless steel (use Type 316 properties)
J-groove weld filler	Alloy 182 [2] (use Alloy 600 properties for SB-167)
J-groove weld butter	Alloy 182 [2] (use Alloy 600 properties for SB-167)

The mechanical and thermal properties for these materials are provided in Section 4.1.1.

C.2.3 Boundary Conditions

The model includes a 180-degree segment of the weld and adjacent portions of the head. The vertical plane containing the vertical axes of the reactor vessel and the outermost penetration forms a plane of symmetry for the model. The displacements normal to this plane of symmetry are fixed (in the global Z-direction). Displacement constraints are also applied to the outer peripheral boundary of the spherical segment to simulate a state of membrane stress. By specifying meridional displacements to be zero in a spherical coordinate system, the head can only displace along a spherical radius parallel to this boundary.

C.3 Finite Element Crack Models

The three-dimensional finite element crack model is developed by removing a portion of the head and butter and inserting a sub-model of crack tip elements, as illustrated in Figure C-2. Displacement constraints are also removed along the plane of symmetry for nodes on the crack face. Figure C-3 shows the final crack model used to analyze a postulated flaw in the J-groove weld and butter.

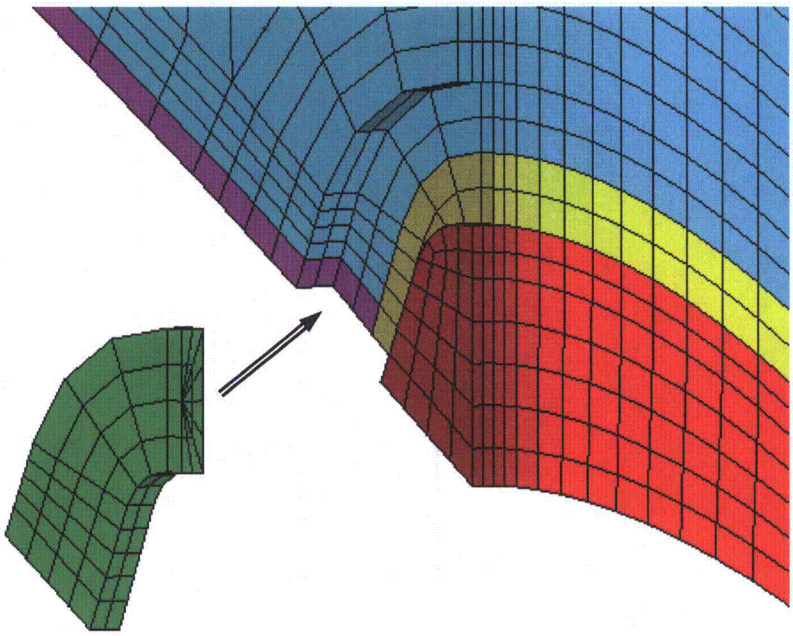

Figure C-2: Development of Crack Model

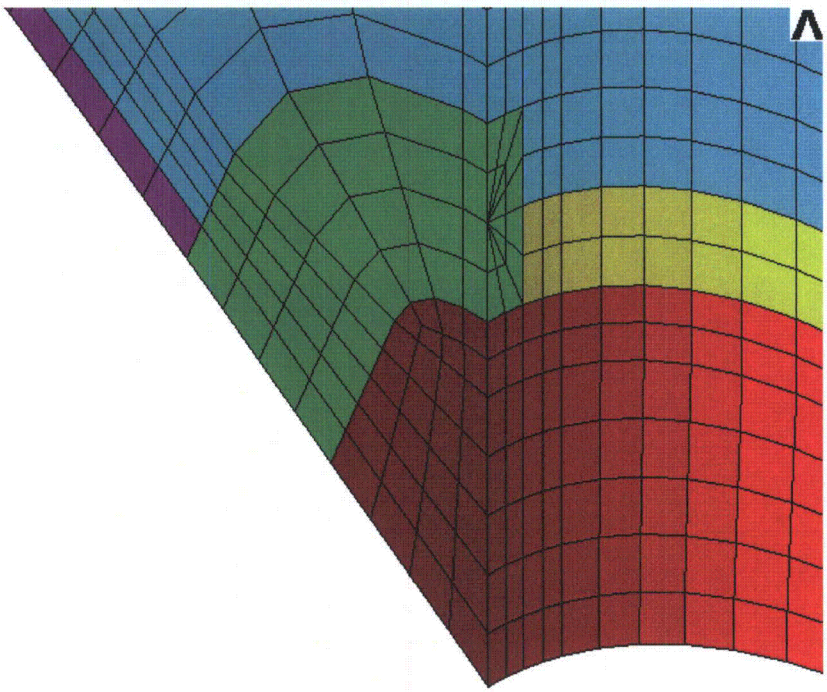

Figure C-3: Final Finite Element Crack Model

APPENDIX D: FINITE ELEMENT STRESS MODEL

A three-dimensional linear-elastic finite element model is developed for use in obtaining operational stresses from transient loading conditions. The origin of this model is the uncracked stress model described in Section C.2, prior to transformation to a crack model. The ANSYS SOLID95 3-D 20-node structural solid elements of the stress model are converted to SOLID90 3-D 20-node thermal solid elements to create a thermal model for use in transient analysis to calculate nodal temperatures.

Three heat transfer regions are defined for applying thermal loads to the model in the form of time-dependent bulk fluid temperatures and convective heat transfer coefficients (HTC). Figure D-1 identifies these regions at the inside surface of the cladding, the bored surface of the head at the location of the nozzle, and the outside surface of the head. Table D-1 lists the bulk fluid temperatures and heat transfer coefficients for the heatup/reactor trip/cooldown full-range transient used in the present flaw evaluations. Table D-2 provides similar data for the rod withdrawal accident transient. Temperature-time history plots are presented in Figure D-2 and Figure D-3 for both transients.

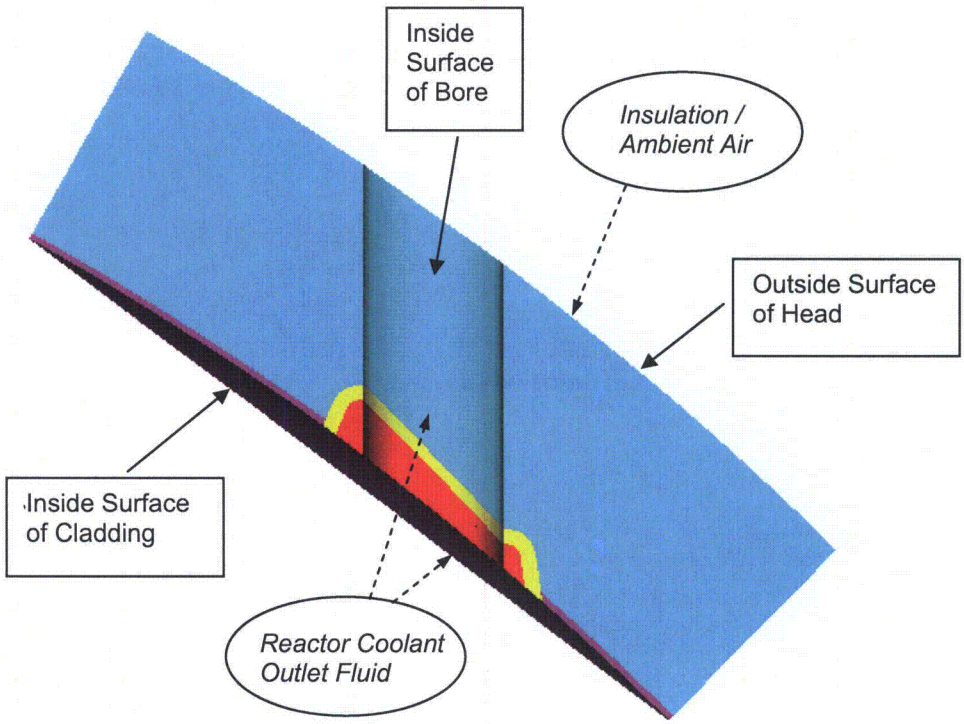

Figure D-1: Heat Transfer Regions of Thermal Model

Table D-1: Heatup/Reactor Trip/Cooldown Transient Definition

References: Section III Stress Analysis [19] and RCS Functional Specification [17]

Load Step	Time (hr.)	Inside Temp. (°F)	Outside Temp. (°F)	Inside Cladding HTC (Btu/hr/in^2-°F)	Inside Bore HTC (Btu/hr/in^2-°F)	Outside Head HTC (Btu/hr/in^2-°F)	Comment
1							
2							
3							heatup
4							
5							
6							SS at 8% power
7							power increase
8							SS at 100% power
9							
10							
11							
12							reactor trip
13							
14							
15							
16							
17							cooldown
18							
19							

Table D-2: Rod Withdrawal Accident Transient Definition

References: Section III Stress Analysis [19] and RCS Functional Specification [17]

Load Step	Time (hr.)	Inside Temp. (°F)	Outside Temp. (°F)	Inside Cladding HTC (Btu/hr/in^2-°F)	Inside Bore HTC (Btu/hr/in^2-°F)	Outside Head HTC (Btu/hr/in^2-°F)	Comment
1							
2							
3							
4							
5							
6							
7							
8							
9							

Figure D-2: Heatup/Reactor Trip/Cooldown Temperature-Time History

Figure D-3: Rod Withdrawal Accident Temperature-Time History

APPENDIX E: STRESS INTENSITY FACTOR DUE TO PRESSURE

The elastic-plastic fracture flaw evaluations of Section 5.3 utilize different safety factors for primary (pressure) and secondary stress (residual and thermal) intensity factors. In order to isolate the pressure term, K_{Ip}, stress intensity factors are developed for an arbitrary pressure load of 2500 psig at 600 °F.

Table E-1 presents stress intensity factors at the ten crack front positions defined in Figure 2-2. Since these values were determined for the initial crack size, they are adjusted by the square root of the crack size, considering the final crack size after four years of crack growth, in the same fashion as described in Section 2.1.3.

The K_{Ip} pressure terms used in the EPFM flaw evaluations of Section 5.3 are derived below.

Let, $$K_{Ip}(a,P) = K_{Ip}(a_o,P_o)\sqrt{\frac{a}{a_o}} \times \frac{P}{P_o}$$

Temperature, $T = 600\ °F$

Pressure, $P_o = 2500$ psig

Initial flaw size, $a_o = 2.035$ in.

From Table E-1, $K_{Ip}(a_o,P_o) = 56.952$ ksi√in

Controlling Transients	Shutdown	Heatup/Cooldown w/ Reactor Trip (RT2)	Rod Withdrawal Accident
Temperature,	T = 70 °F	{ } °F	{ } °F
Pressure,	P = 0 psig	{ } psig	{ } psig
Final flaw size,	a = 2.1048 in.	2.1048 in.	2.1048 in.
Final stress intensity factor,	$K_{Ip}(a,P)$ = 0 ksi√in	39.849 ksi√in	63.597 ksi√in

Table E-1: Stress Intensity Factors for Internal Pressure Loading

Temperature =	600	F
Pressure =	2500	psig
Flaw size =	2.035	in.

	Position	SIF (ksi√in)
Inside Surface	1	56.697
	2	51.258
	3	49.563
	4	48.028
	5	46.116
	6	43.286
	7	39.883
	8	41.978
	9	50.267
Bored Surface	10	56.952

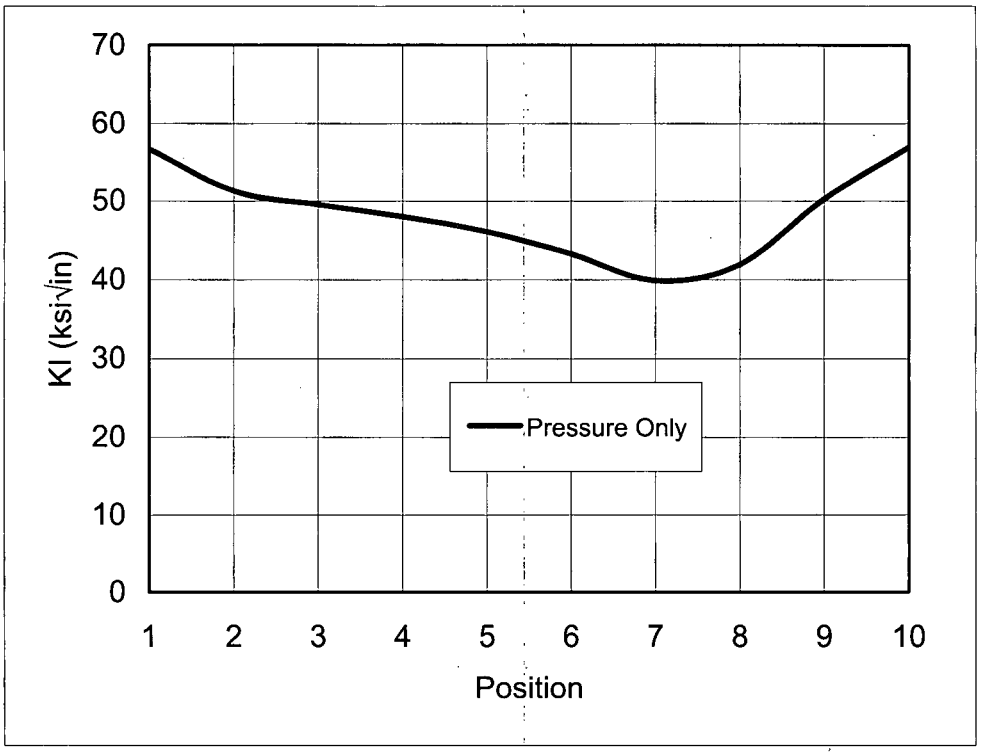

Enclosure B
L-10-131

Affidavit for DB-1 CRDM Nozzle J-Groove Weld Flaw Evaluation for IDTB Repair
(3 pages follow)

AFFIDAVIT

COMMONWEALTH OF VIRGINIA)
) ss.
CITY OF LYNCHBURG)

1. My name is Gayle F. Elliott. I am Manager, Product Licensing, for AREVA NP Inc. and as such I am authorized to execute this Affidavit.

2. I am familiar with the criteria applied by AREVA NP to determine whether certain AREVA NP information is proprietary. I am familiar with the policies established by AREVA NP to ensure the proper application of these criteria.

3. I am familiar with the AREVA NP information contained in Calculation Summary Sheet (CSS) 32-9134664-002 entitled "DB-1 CRDM Nozzle J-Groove Weld Flaw Evaluation for IDTB Repair," dated April 2010 and referred to herein as "Document." Information contained in this Document has been classified by AREVA NP as proprietary in accordance with the policies established by AREVA NP for the control and protection of proprietary and confidential information.

4. This Document contains information of a proprietary and confidential nature and is of the type customarily held in confidence by AREVA NP and not made available to the public. Based on my experience, I am aware that other companies regard information of the kind contained in this Document as proprietary and confidential.

5. This Document has been made available to the U.S. Nuclear Regulatory Commission in confidence with the request that the information contained in this Document be withheld from public disclosure. The request for withholding of proprietary information is made in accordance with 10 CFR 2.390. The information for which withholding from disclosure is

requested qualifies under 10 CFR 2.390(a)(4) "Trade secrets and commercial or financial information."

6. The following criteria are customarily applied by AREVA NP to determine whether information should be classified as proprietary:

(a) The information reveals details of AREVA NP's research and development plans and programs or their results.

(b) Use of the information by a competitor would permit the competitor to significantly reduce its expenditures, in time or resources, to design, produce, or market a similar product or service.

(c) The information includes test data or analytical techniques concerning a process, methodology, or component, the application of which results in a competitive advantage for AREVA NP.

(d) The information reveals certain distinguishing aspects of a process, methodology, or component, the exclusive use of which provides a competitive advantage for AREVA NP in product optimization or marketability.

(e) The information is vital to a competitive advantage held by AREVA NP, would be helpful to competitors to AREVA NP, and would likely cause substantial harm to the competitive position of AREVA NP.

The information in the Document is considered proprietary for the reasons set forth in paragraphs 6(b) and 6(c) above.

7. In accordance with AREVA NP's policies governing the protection and control of information, proprietary information contained in this Document have been made available, on a limited basis, to others outside AREVA NP only as required and under suitable agreement providing for nondisclosure and limited use of the information.

8. AREVA NP policy requires that proprietary information be kept in a secured file or area and distributed on a need-to-know basis.

9. The foregoing statements are true and correct to the best of my knowledge, information, and belief.

SUBSCRIBED before me this 20th

day of April 2010.

Sherry L. McFaden
NOTARY PUBLIC, COMMONWEALTH OF VIRGINIA
MY COMMISSION EXPIRES: 10/31/10
Reg. # 7079129

SHERRY L. MCFADEN
Notary Public
Commonwealth of Virginia
7079129
My Commission Expires Oct 31, 2010